ANL/ESD/TM-82

Geophysical Exploration in the Lautertal at the Combat Maneuver Training Center, Hohenfels, Germany

Energy Systems Division
Argonne National Laboratory

Operated by The University of Chicago,
under Contract W-31-109-Eng-38, for the
United States Department of Energy

TJ

Argonne National Laboratory

Argonne National Laboratory, with facilities in the states of Illinois and Idaho, is owned by the United States Government, and operated by the University of Chicago under the provisions of a contract with the Department of Energy.

This technical memo is a product of Argonne's Energy Systems (ES) Division. For information on the division's scientific and engineering activities, contact:

Director, Energy Systems Division
Argonne National Laboratory
Argonne, Illinois 60439-4815
Telephone (708) 252-3724

Presented in this technical memo are preliminary results of ongoing work or work that is more limited in scope and depth than that described in formal reports issued by the ES Division.

Publishing support services were provided by Argonne's Information and Publishing Division.

Disclaimer

Reproduced directly from the best available copy.

Available to DOE and DOE contractors from the Office of Scientific and Technical Information, P.O. Box 62, Oak Ridge, TN 37831; prices available from (615) 576-8401.

Available to the public from the National Technical Information Service, U.S. Department of Commerce, 5285 Port Royal Road, Springfield, VA 22161.

DISCLAIMER

Portions of this document may be illegible in electronic image products. Images are produced from the best available original document.

ANL/ESD/TM-82

Geophysical Exploration in the Lautertal at the Combat Maneuver Training Center, Hohenfels, Germany

by P.C. Heigold, M.D. Thompson, and H.M. Borden

Center for Environmental Restoration Systems, Energy Systems Division,
Argonne National Laboratory, 9700 South Cass Avenue, Argonne, Illinois 60439

October 1994

Work sponsored by United States Department of Defense, United States Army, Europe, Combat Maneuver Training Center, Hohenfels, Germany

Contents

Tables

Figures

Figures (Cont.)

Figures (Cont.)

Geophysical Exploration in the Lautertal at the Combat Maneuver Training Center, Hohenfels, Germany

by

P.C. Heigold, M.D. Thompson, and H.M. Borden

Abstract

Geophysical exploration was conducted in the Lautertal at the Combat Maneuver Training Center, Hohenfels, Germany, to determine the shallow geological framework of a typical dry valley in this karstic environment. The complementary methods of electromagnetic surveying, vertical electrical soundings, and seismic refraction profiling were successful in determining the depth and configuration of the bedrock surface, the character of the unconsolidated deposits resting on the bedrock surface, and the nature of the bedrock surface. Channels and other depressions in the bedrock surface are aligned with structurally induced fractures in the bedrock. The unconsolidated deposits consist of coarse alluvium and colluvium, which are confined to these channels and other depressions, and fine-grained loam and loess, which cover most of the Lautertal. Wide ranges in the electrical and elastic parameters of the bedrock surface are indicative of carbonate rock that is highly fractured and dissolved at some locations and competent at others. Most local groundwater recharge occurs in the uplands where the Middle Kimmeridge (Delta) Member of the Malm Formation (Jurassic) is widely exposed. These carbonate rocks are known to be susceptible to dissolution along the fractures and joints; thus, they offer meteoric waters ready access to the main shallow aquifers lower in the Malm Formation. These same rocks also form the bedrock surface below many of the dry valleys, but in the Lautertal, the infiltration of meteoric waters into the subsurface is generally impeded by the surficial layer of fine-grained loam and loess, which have low hydraulic conductivity. Further, the rocks of the Middle Kimmeridge Member appear to be closely associated with the localized occurrence of turbidity in such perennial streams as the Lauterach.

1 Introduction

The environmental management office at the Combat Maneuver Training Center, Hohenfels, Germany, would like to ensure that military impacts on local groundwater quality and flow are minimized or eliminated. In order to accomplish this goal, a valid model of the groundwater flow system, along with a geographic information system to facilitate data input and output, is needed for planning and response purposes.

Conceptual and numerical groundwater flow models of the Combat Maneuver Training Center and its surroundings must be based on a thorough knowledge of geologic and hydrologic conditions in the Hohenfels region. Much of this information can be obtained through a series of basic geophysical and hydrogeological investigations.

Geophysical exploration was conducted in the Lautertal at the Combat Maneuver Training Center (Figures 1 and 2) to determine the shallow geological framework of a typical "dry" valley in this karstic environment. The term dry, as used here, implies well-drained without perennial streams. Knowledge of the shallow geological framework of these numerous dry valleys is essential to understanding the roles of these valleys in the shallow groundwater flow system.

Groundwater in the shallow aquifers of this region is highly susceptible to contamination from surficial sources as a result of the high degree of interdependency between surficial drainage and subsurface flow. Even the deeper, regional, water-supply aquifers are at risk from contamination unless they are separated from the shallow aquifers by geological units with very low hydraulic conductivities.

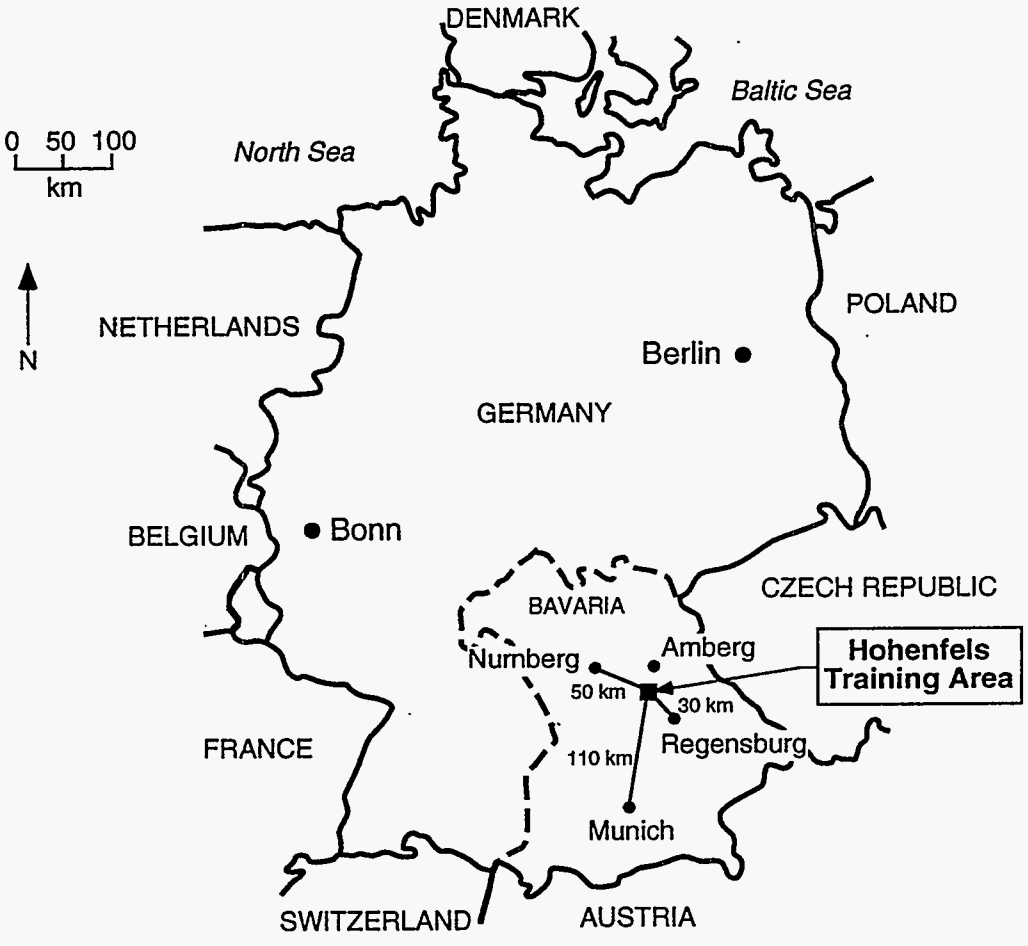

FIGURE 1 Location of Hohenfels Training Area in Germany

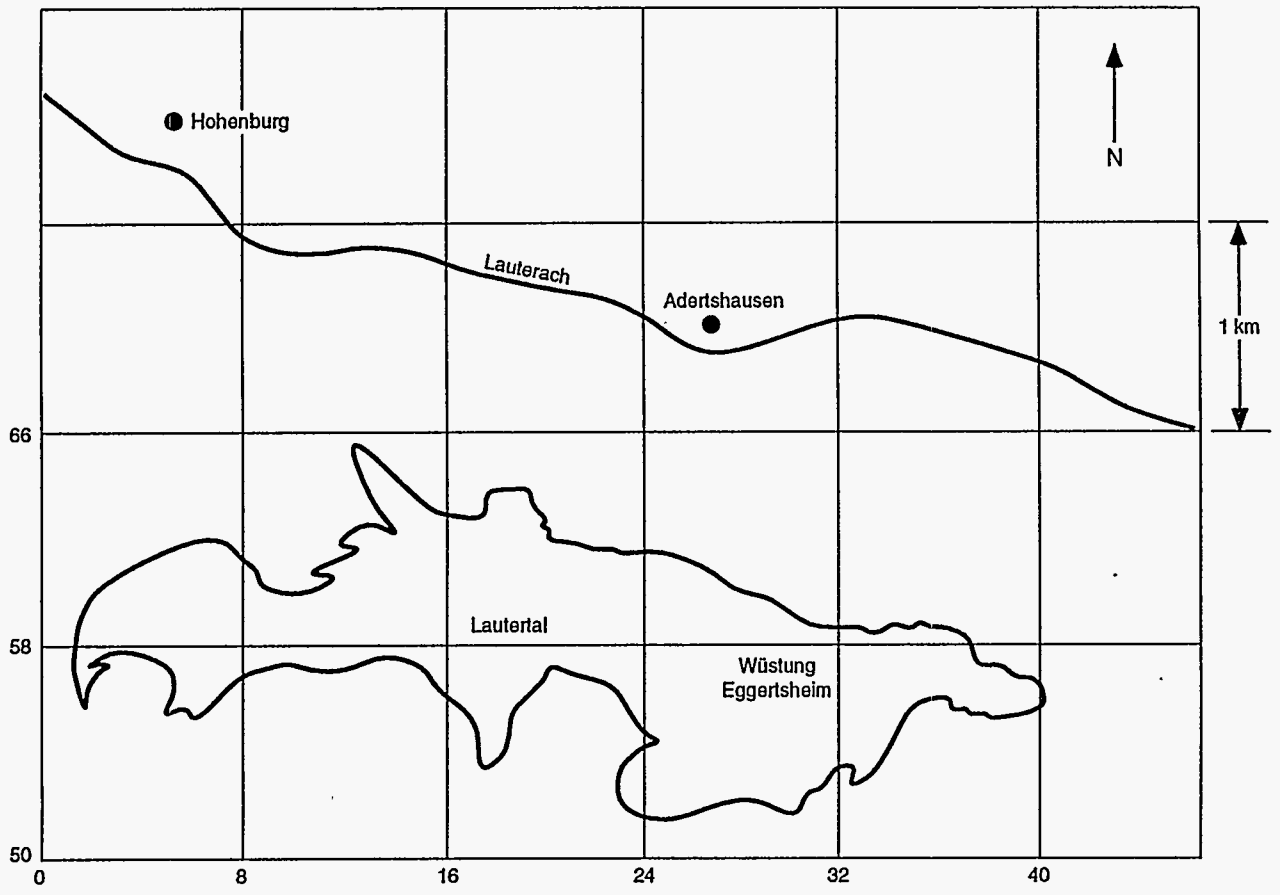

FIGURE 2 Map of the Lautertal Study Area Covered by an Orthogonal Grid

In the Hohenfels region, heavy rainfall is often immediately followed by localized occurrences of increasing turbidity in some perennial rivers and streams that are independent from tributary influences. This situation would suggest that residence time of water in the shallow aquifers is short and that pathways from points of recharge to points of discharge may be relatively simple.

Geophysical exploration in a well-developed karstic environment can be difficult. Interfaces between geological units can be quite irregular. Fracturing and dissolution of the carbonate rocks can, and often do, alter the magnitudes of geophysical parameters that are normally expected from these lithotypes. The success of a geophysical exploration program in such an environment depends on the selection of appropriate geophysical methods and the careful interpretation of data. Although individual methods may have shortcomings, the chosen methods must complement one another in such a way as to collectively provide diagnostic results.

A geophysical exploration program specifically designed for the Lautertal project consisted of electromagnetic surveying, vertical electrical soundings, and seismic refraction profiling. These geophysical techniques were chosen to provide information on the depth and configuration of the bedrock surface, the nature of the unconsolidated deposits resting on the bedrock surface, and the character of the bedrock. This information is required to create conceptual and numerical hydrogeological models of the groundwater flow system.

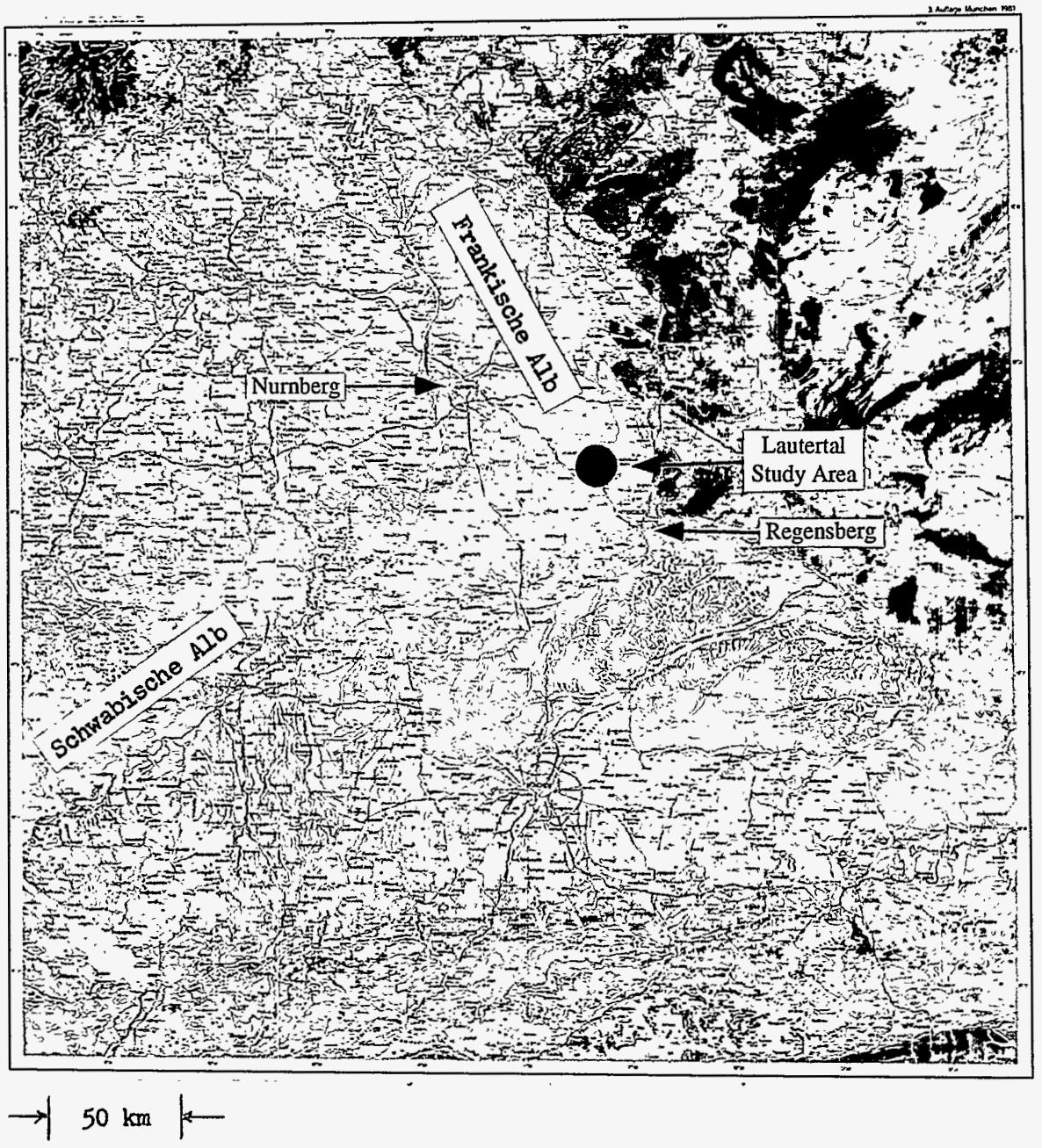

FIGURE 3 Geologic Map of Bavaria

2 Geological Setting

The Lautertal study area is located in the southeastern part of the Frankische Alb, a continuation of the Schwabische Alb (Figure 3). In this region, the countless, forested, dolomitic knolls on the flanks of deep valleys like the Lautertal form an imposing karstic landscape. The upper bedrock units in the Lautertal are composed of reef dolomite and limestones of the Middle Kimmeridge (Delta) Member of the Malm Formation (Jurassic) (Meyer 1990) (Figures 4 and 5). Within the Lautertal, there are remnants of what are believed to be Upper Cretaceous rocks (Schutzfelsschichten or protective rock layers). These deposits are mainly fluvial, and they lie in channels and other depressions on the bedrock surface, the result of dissolution along joints and fractures that began early in Cretaceous time (Meyer 1990). Undifferentiated Pleistocene and Recent deposits, loam and loess over limestone and dolomitic rubble, blanket the Lautertal valley and its tributary valleys, except for a small area at the west end of the Lautertal where the Schutzfelsschichten is exposed. The erosion-resistant knolls that flank the Lautertal are composed of reef dolomite and layers of the Upper Kimmeridge (Epsilon) Member of the Malm Formation (Meyer 1990).

The varying resistance of the Malm to erosion and the susceptibility of this formation to dissolution have been cited as the factors responsible for the present topography in the Lautertal region (Meyer 1990). The thinly bedded facies of the Malm, a sequence of limestones and marly limestones that have been differentially dolomitized, is generally more resistant to erosion. The massive limestone facies, which consists primarily of dolomitized coralline reef with sponges and brachiopods, is more susceptible to dissolution. As in other karstic carbonate terrains in temperate climates, the occurrence of fractures is believed to contribute significantly to the development of dissolution features (Lattman and Parizek 1964).

Regionally, the Malm Formation rests on the Dogger Formation (Jurassic). The Dogger is composed mainly of sandstones, shales, and marls. The uppermost member of the Dogger Formation, the Zeta Member, contains the Ornaten clay. The Ornaten clay is important because it forms the lower confining layer of the Malm aquifer, the principal shallow aquifer in the region.

Bedrock strata in the Lautertal dip gently to the east, toward the Riedener-Kallmünzer Ast, a branch of the Frankische Mulde (trough) (Freyberg 1969) (Figure 6). There are no major faults or folds in the Lautertal region. Fuhrmann (1967) examined several small bedrock structures in the area, including some at nearby Stettkirchen, and concluded that the principal directions of fractures and joints in the bedrock are north-northeast and west-northwest.

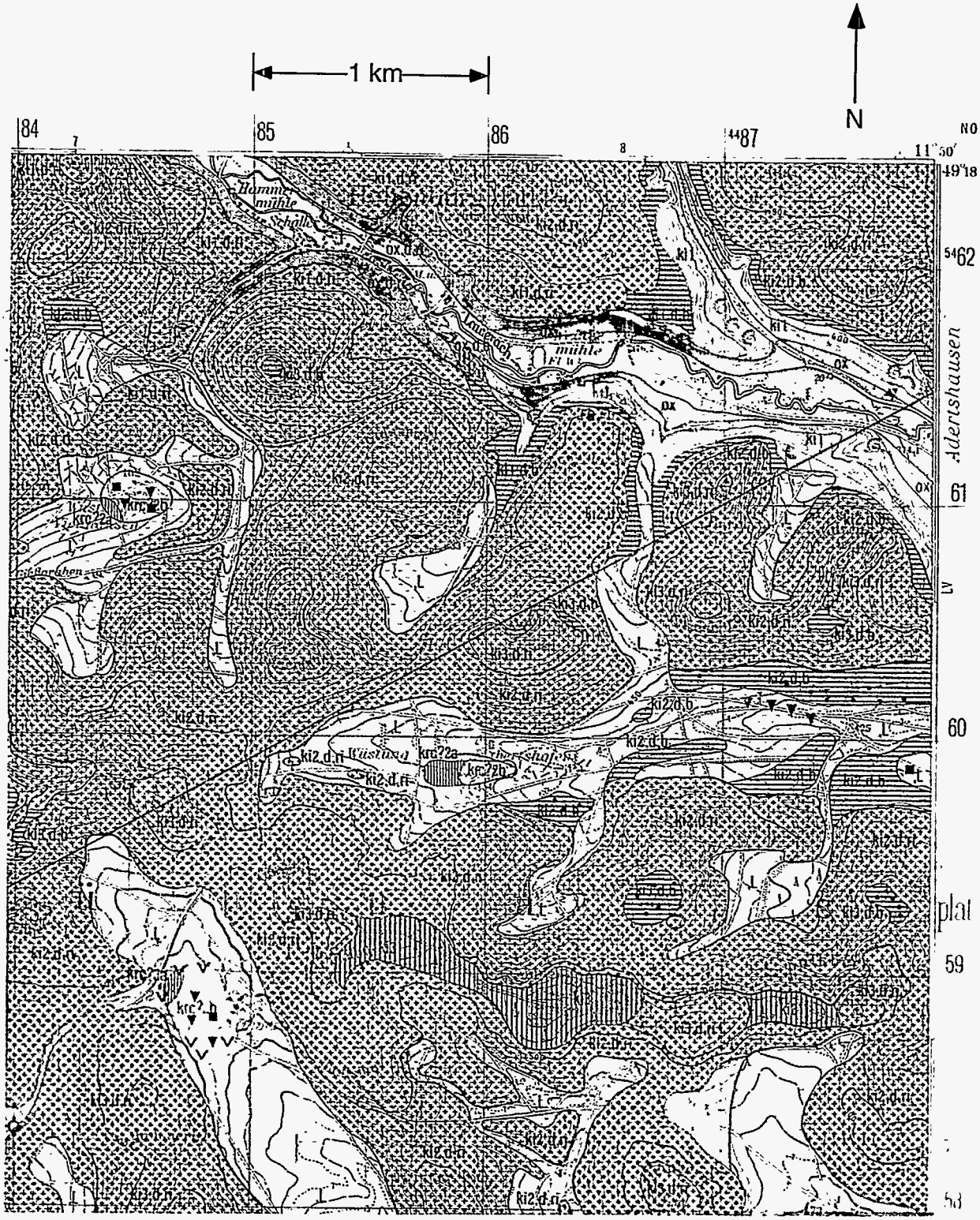

FIGURE 4 Geologic Map of the Lautertal Region (Velburg Quad)

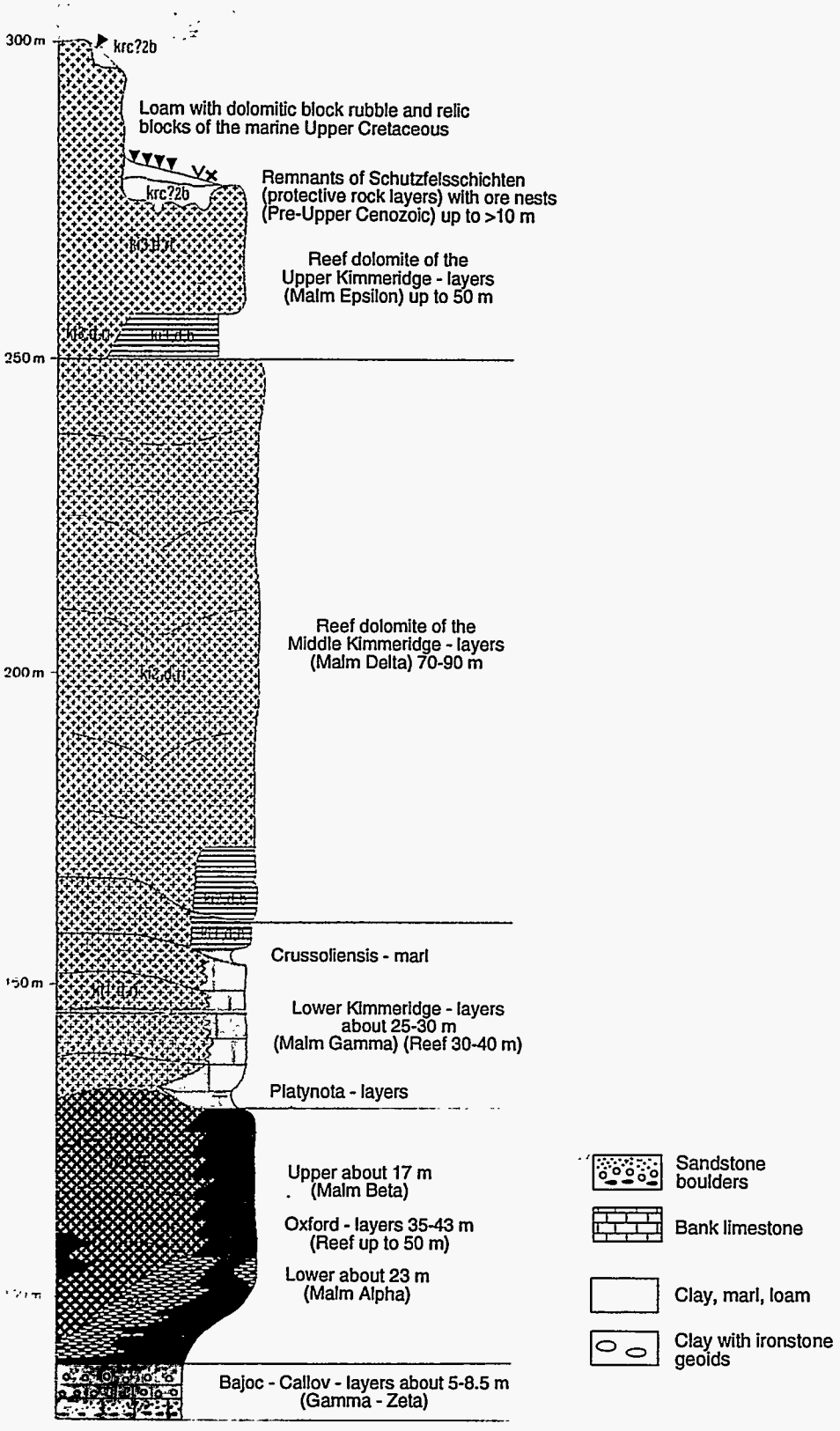

FIGURE 5 Columnar Section from the Earth's Surface to the Gamma-Zeta Members of the Dogger Formation (Jurassic)

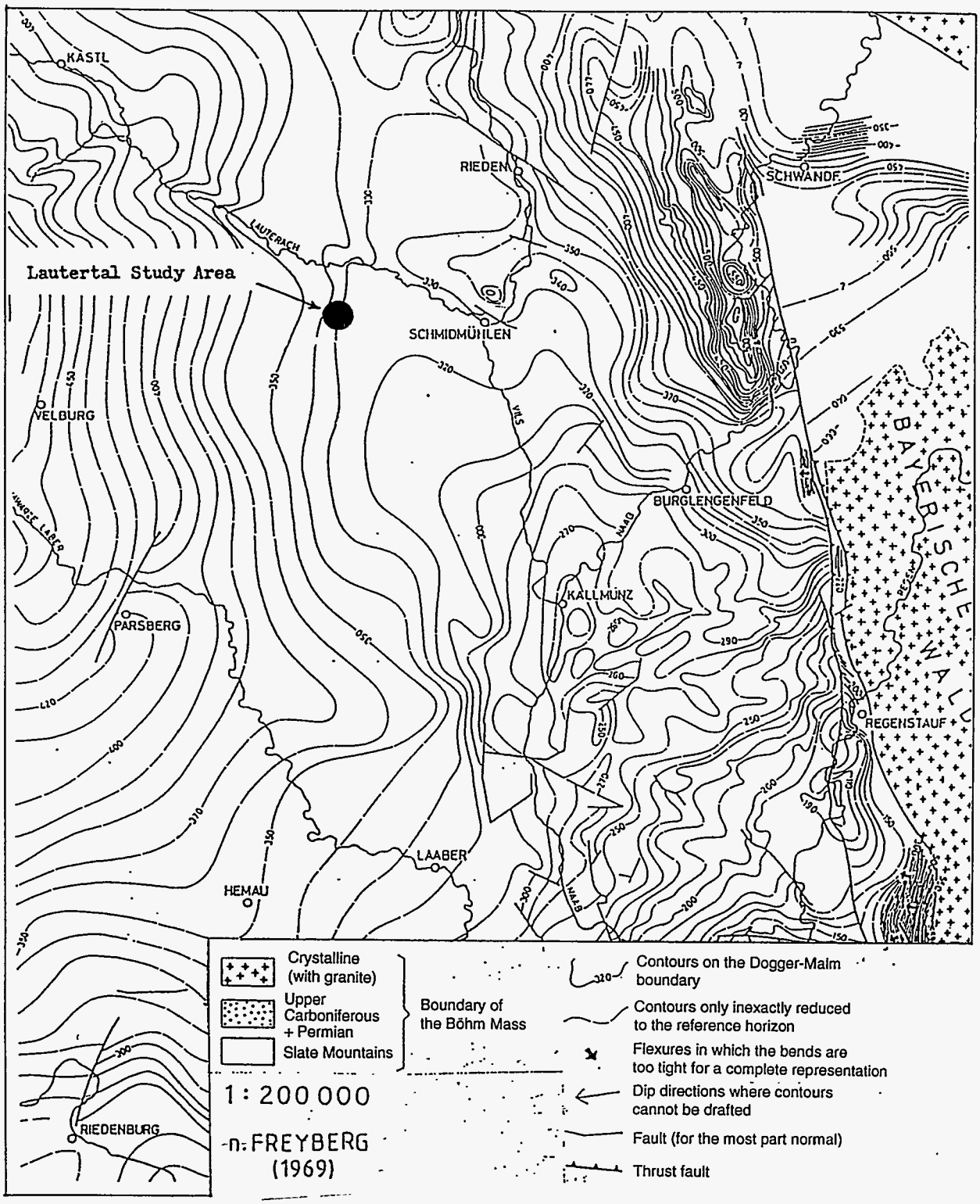

FIGURE 6 Structure on the Top of the Dogger Formation (Jurassic) (Adapted from Freyberg, 1969)

3 Hydrogeology

The hydrogeology of the Lautertal study area is typical of a karstic environment. The trellis/rectangular drainage pattern that has developed on the surface is indicative of structurally controlled topography and drainage (Figure 4). Valleys and ephemeral streams tend to form above solution-widened joints and fractures in the bedrock. Joints and fractures in the bedrock surface serve as receiving points for water and contaminants infiltrating through the vadose zone.

In such dry valleys as the Lautertal, where the joints and fractures at the bedrock surface have become sizable channels and depressions, the vadose zone may include surficial loam and loess, alluvium and colluvium, and a portion of the upper bedrock. The alluvial and colluvial deposits are a combination of the Schutzfelsschichten (Upper Cretaceous) and coarse Pleistocene and Recent deposits. The coarse deposits resting on the bedrock surface have hydraulic conductivities much greater than those of the fine-grained loam and loess. Still in the valley, but away from the channels and other depressions in the bedrock surface, the alluvial and colluvial deposits may be absent, and the vadose zone may include only surficial loam and loess and a portion of the upper bedrock. In the uplands, away from the valleys, the vadose zone consists of only the upper bedrock, which is exposed at the earth's surface.

The principal near-surface aquifer in the Lautertal region is a network of joints, fractures, and cavities in the carbonate Malm Formation (Jurassic). The joints, fractures, and cavities are the result of tectonic stresses and subsequent dissolution. In a region of moderate rainfall, the development of fracture porosity through solution occurs rapidly in the tens of meters immediately below the bedrock surface, where the groundwater flow system is open and accessible to rapid recharge. Rainfall and evaporation in the Lautertal region at the present time have been estimated to be approximately 700 and 480 mm/yr, respectively (Schoger 1992).

In places the Malm aquifer is confined (Ebasco-Dorch Consultants, Inc. 1990). Under these conditions, the upper confining layer consists of dense, dolomitic limestone, also of the Malm Formation. The lower confining layer is the Ornaten clay of the Zeta Member of the Dogger Formation. When the top of the Malm aquifer was breached during drilling at the Old Landfill about 4 km south of the Lautertal, the water rose in the well bores approximately 20 m, indicating a very impermeable upper confining layer (Schoger 1992). In the area of the Old Landfill, the Malm aquifer was estimated to be 70-80 m thick, and the depth to the top of the aquifer was approximately 61 m. Borings at the Old Landfill confirmed an exceptionally thick unsaturated zone above the Malm aquifer (45-61 m). There are reasons to believe that similar conditions exist in the Lautertal. The near-surface geology in the Lautertal is essentially the same as that at the Old Landfill. Unconsolidated deposits consisting of loam and loess over limestone and dolomitic rubble rest on carbonate rocks of the Middle Kimmeridge Member of the Malm Formation (Meyer 1990). Surface elevations at the Old Landfill are similar to those in the center of the Lautertal directly to the north. A water-table elevation map of Bavaria (Andres and Wirth 1985) shows similar elevations at both locations.

The lowest surface elevations in the Lautertal are located in a north-south valley that transects the Lautertal near the western side of Wüstung Eggertsheim (Figure 2). Runoff of meteoric waters that do not infiltrate the vadose zone accumulate in this valley before flowing northward into the Lauterach. Some ponding occurs at localized low spots in the relatively impermeable, fine-grained surficial deposits.

The meteoric waters that infiltrate the vadose zone and ultimately find their way to the main Malm aquifer flow eastward and southeastward toward the Vils and Naab Rivers (Andres and Wirth 1985) (Figures 7 and 8).

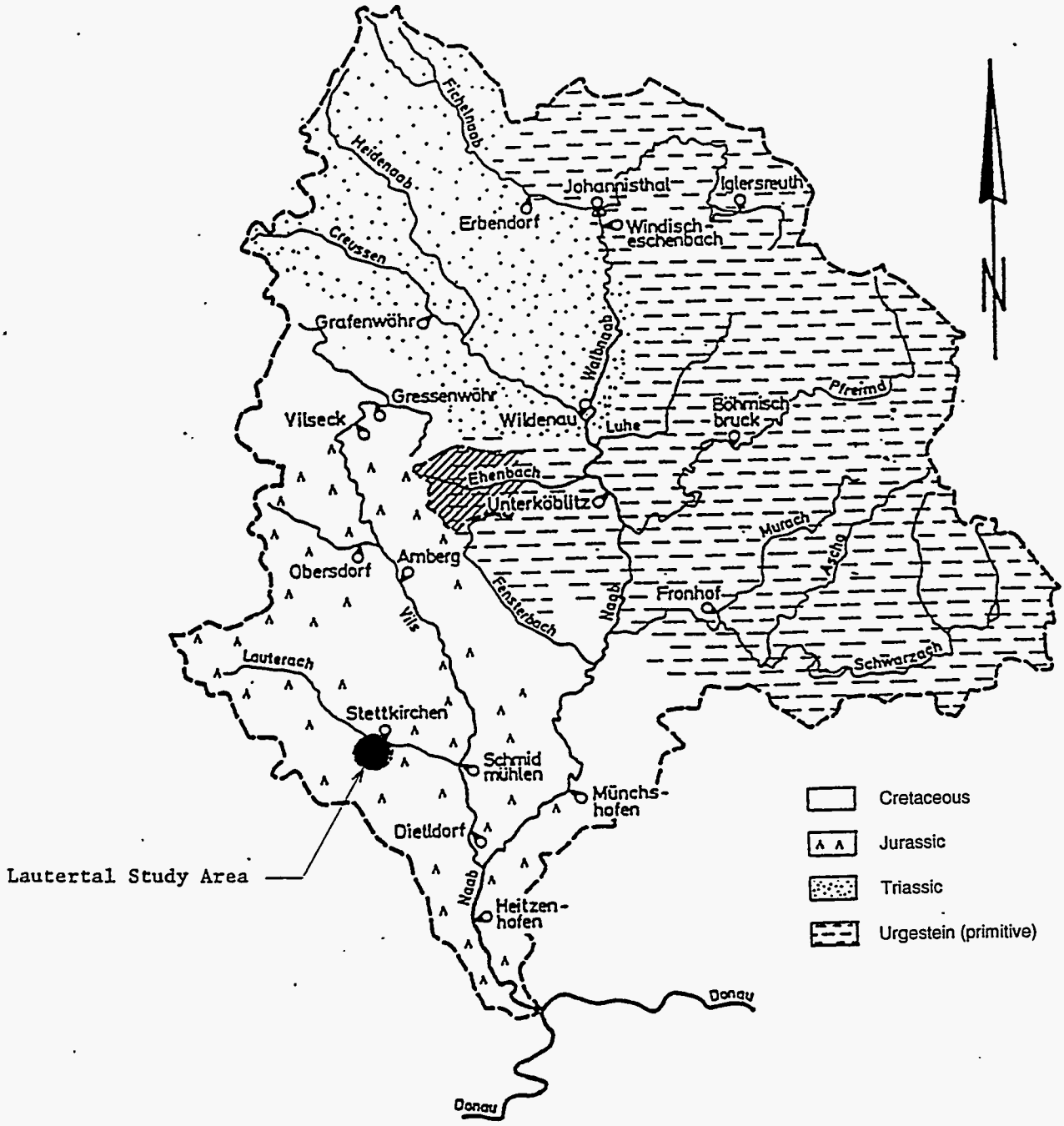

FIGURE 7 Drainage Basin of the Naab River

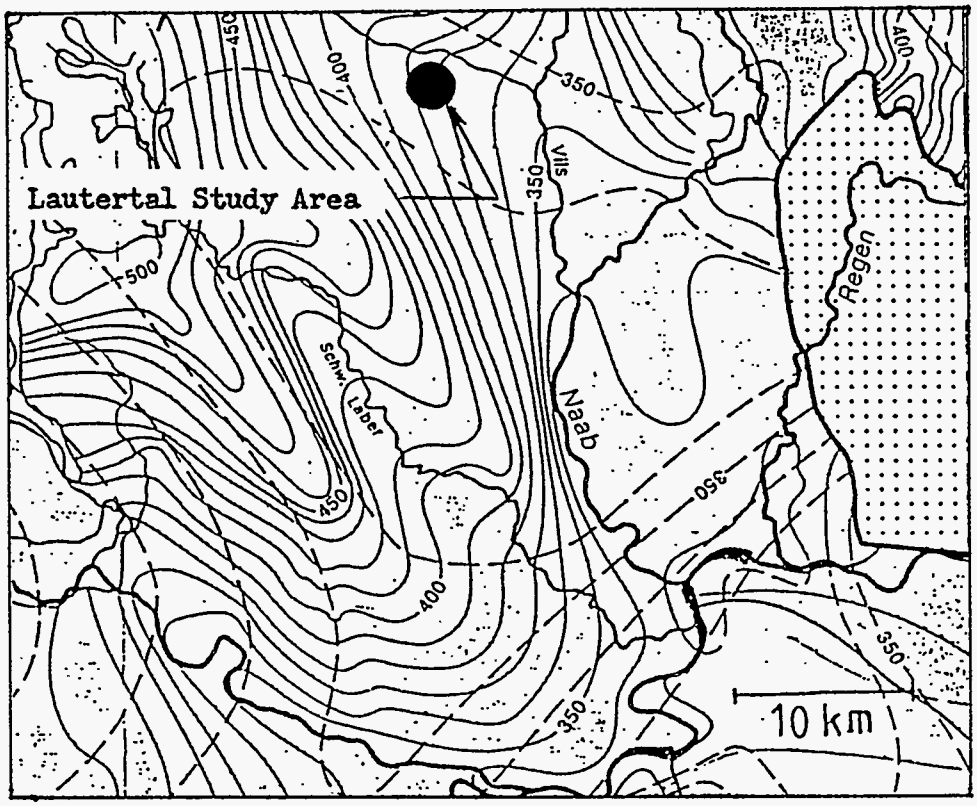

FIGURE 8 Water-Table Elevations in Bavaria (Adapted from Andres and Wirth, 1985)

4 Geophysical Exploration

4.1 Land Surveying

In order to facilitate the collection, reduction, and interpretation of geophysical data, an orthogonal grid was established over the Lautertal by Wolf-Blumenthal Ingenieurbüro, Nürnberg (see Figure 2). The lines of this grid were oriented in north-south and east-west directions, and nodal spacing was 0.125 km. The locations of the nodes were accurate to 1.0 m in the horizontal and 0.1 m in the vertical (see Table A.1 in Appendix A). A computer-generated surface topography map of the study area, based on nodal elevations, is shown in Figure 9. All but a few of the geophysical measurements made in this study were located at nodes or along lines of the orthogonal grid.

4.2 Electromagnetic Surveying

Electromagnetic surveying provided a rapid, qualitative examination of the electrical properties (conductivity) of the near-surface deposits in the Lautertal study area. Electromagnetic readings were made with a Geonics EM-34 instrument at 220 nodes of the orthogonal grid covering the Lautertal study area. At each node, three apparent conductivity values (in millimhos/meter) were obtained by holding the transmitting and the receiving coils on the earth's surface in the same vertical plane (horizontal dipoles) at spacings of 10, 20, and 40 m (see Table A.2). The apparent conductivity values represent weighted averages of the conductivities of the rocks between the transmitter and the receiver. The conductivities of the rocks near the earth's surface are weighted most heavily, and the depth of investigation is generally some fraction of the spacing between the transmitter and the receiver. This fraction is dependent on the conductivities of the rocks. Increasing the spacing between the transmitter and the receiver increases the depth of investigation (Telford et al. 1976).

In this study, the apparent conductivity values ranged from 0.1 to 29.0 mmho/m. The largest values are associated with fine-grained unconsolidated deposits (loam and loess). The intermediate values are generally associated with coarse unconsolidated deposits (alluvium and colluvium) and perhaps fractured and/or dissolved carbonate bedrock. The smallest conductivity values are associated with competent carbonate bedrock.

Areal distributions of apparent conductivity in the Lautertal corresponding to transmitter-receiver spacings of 10, 20, and 40 m are shown in Figures 10, 11, and 12, respectively. (Other visualizations of the electrical conductivity distributions are shown in Appendix B, Figure B.1.) At all three spacings, the largest apparent conductivity values appear to be collocated along distinct north-south and east-west linear trends. Further, as the transmitter-receiver spacing increases and the depth of investigation also increases, the width of these trends and the largest apparent conductivity values within these trends decrease. These observations indicate the presence of

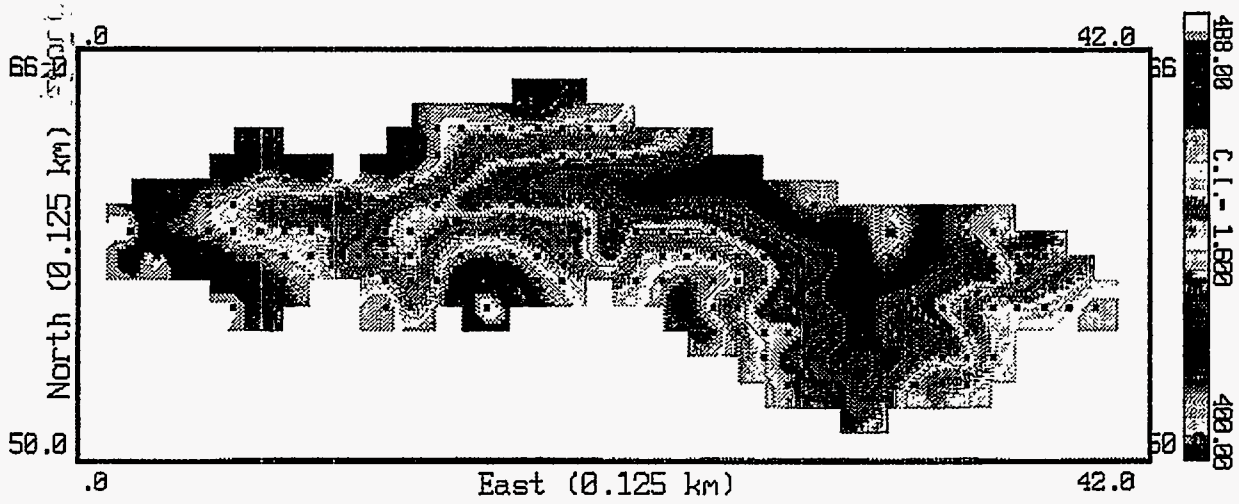

FIGURE 9 Surface Topography of the Lautertal Study Area

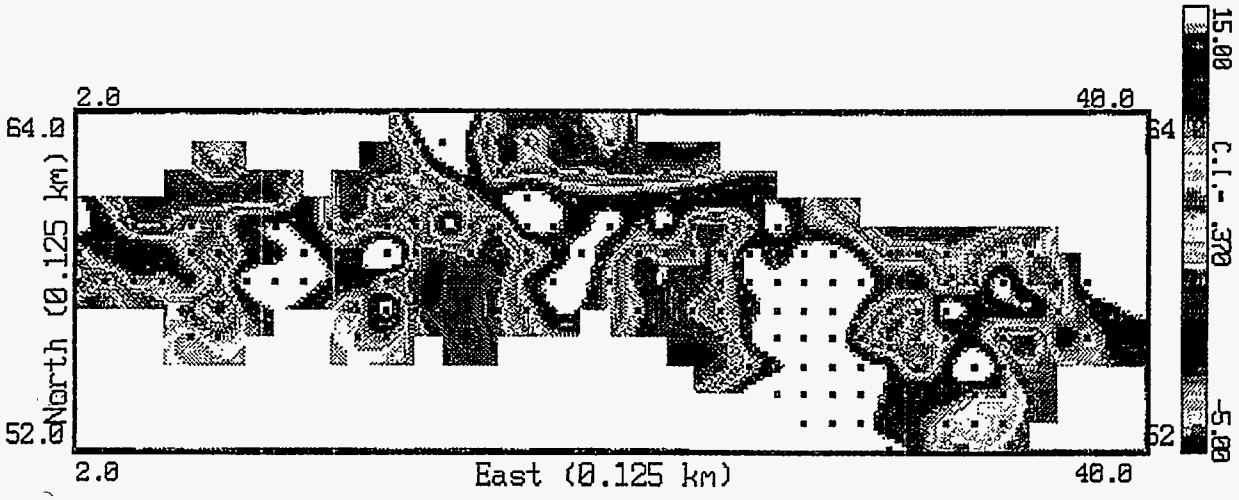

FIGURE 10 Areal Distribution of Apparent Conductivity as Determined by Electromagnetic Surveying with a 10-m Transmitter-Receiver Spacing

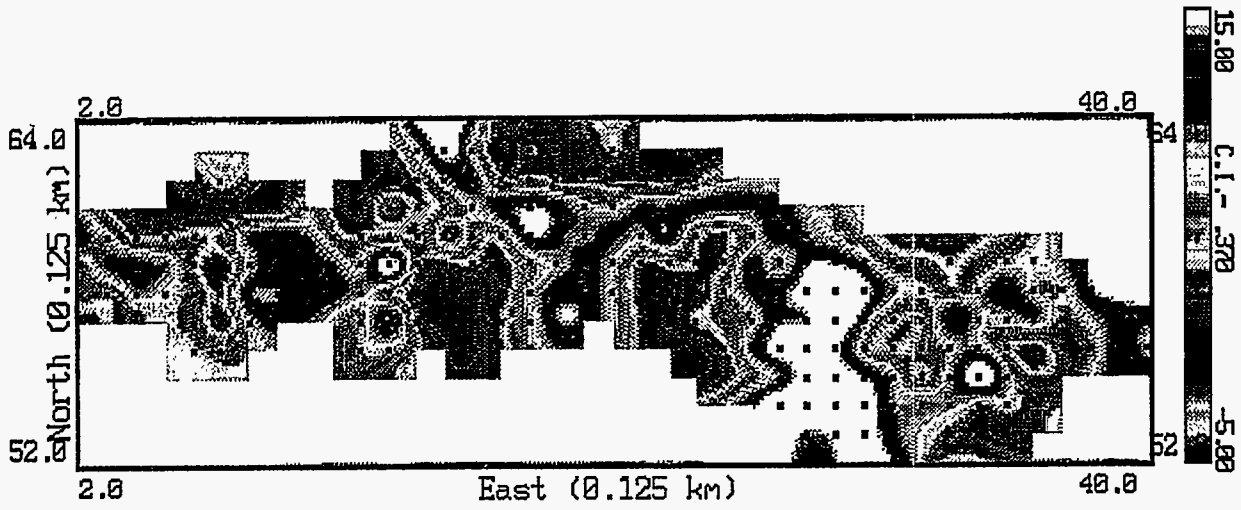

FIGURE 11 Areal Distribution of Apparent Conductivity as Determined by Electromagnetic Surveying with a 20-m Transmitter-Receiver Spacing

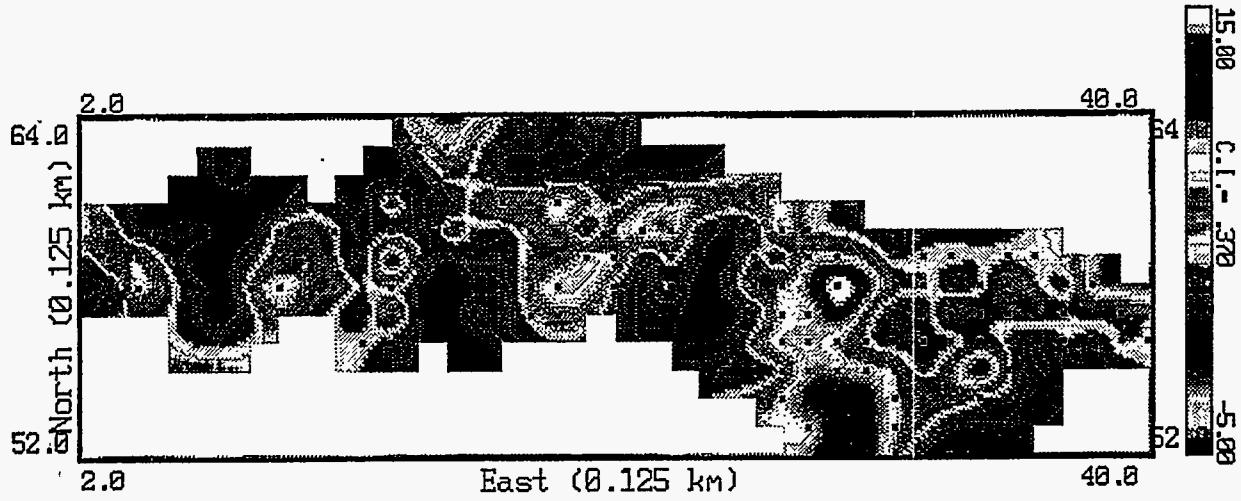

FIGURE 12 Areal Distribution of Apparent Conductivity as Determined by Electromagnetic Surveying with a 40-m Transmitter-Receiver Spacing

channels and other depressions on the bedrock surface that have been filled with unconsolidated deposits — first, generally coarse alluvium and colluvium, then, fine-grained loam and loess. These latter deposits blanket most of the Lautertal, but they may reach their greatest thickness above channels and other depressions in the bedrock surface that have not been completely filled with alluvium and colluvium. The fact that the width and amplitudes of the high apparent conductivity trends are greatly reduced in Figure 12 indicates that the maximum depths of the channels and other depressions in the bedrock surface are approximately 40 m.

According to the electromagnetic data, the main channel in the bedrock surface is relatively broad and transects the Lautertal in an approximate north-south direction near the west side of Wüstung Eggertsheim (north-south grid line 29). The loci of the lowest surface elevations in the Lautertal lie almost directly above this main channel in the bedrock surface (Figure 9). Smaller channels in the bedrock surface that roughly parallel the axis of the Lautertal, and that have tributaries of their own, join the main channel in the bedrock surface from the east and from the west.

4.3 Vertical Electrical Soundings

Vertical electrical soundings provided a "quantitative" examination of the electrical properties (resistivity, the reciprocal of conductivity) of the near-surface deposits in the Lautertal study area. The term quantitative, as used here, indicates that the data acquired by using this method were able to be inverted to layering parameters (resistivities and thicknesses). While it may appear that there was a redundancy in employing this geophysical method in addition to electromagnetic surveying, because both methods essentially measure the same geophysical parameter, the fact is that these two methods complement each other. The vertical electrical soundings serve to constrain the qualitative, but more voluminous, electromagnetic data.

Vertical electrical soundings were made with an ABEM Terrameter System, Model SAS 300C, at 147 nodes of the orthogonal grid covering the Lautertal. At each station, a-spacings of a Wenner electrode configuration were expanded in appropriate increments to provide a smooth, yet detailed, curve of apparent resistivity (in ohm-meters) versus a-spacing (in meters). Maximum a-spacings were usually 120 m.

The apparent resistivity values obtained in vertical electrical soundings represent weighted averages of the resistivities of the rocks between the potential surfaces that intersect the earth's surface at the potential (inner) electrodes of the Wenner electrode configuration. The resistivities of the rocks near the earth's surface are weighted most heavily, and the depth of investigation is generally some fraction of the distance between the potential electrodes (which is also the a-spacing). Increasing the a-spacing increases the depth of investigation.

Apparent resistivity versus a-spacing curves were inverted to layering parameters (resistivities and thicknesses) by using the commercially available software package, Resix Plus (Table A.3). Resix Plus assumes that the observed apparent resistivity versus a-spacing curves

are the result of a series of horizontal layers below the center point of the Wenner electrode configuration.

Inversion of the vertical electrical sounding data gathered in the Lautertal provided information about three near-surface layers of rock. In descending order, these layers correspond to the fine-grained loam and loess, the generally coarse alluvial and colluvial deposits, and the carbonate bedrock. A three-dimensional view of the shallow geological framework of the Lautertal as determined by vertical electrical soundings, is shown in Figure B.2. As indicated in Section 2, in the Lautertal, away from the channels and depressions in the bedrock surface, the middle layer of alluvial and colluvial deposits is absent. The carbonate bedrock surface may be highly fractured and/or dissolved or quite competent. Coarse alluvial and colluvial deposits can have resistivity values quite similar to those of highly fractured and dissolved carbonate rock. Thus, when these two rock types are juxtaposed, the location of their interface is often difficult to determine on the basis of vertical electrical sounding data. Occasionally, the inversion of the vertical electrical sounding data provided layering solutions consisting of more than three layers. Although such layering solutions are geologically feasible, such solutions may result from errors introduced during the acquisition of the data. For example, abrupt changes in elevations of the earth's surface encountered during the expansion of the Wenner electrode configuration may have caused "noise" in the acquired data. Such conditions were noted during the data acquisition, and inversions of data gathered under such conditions were viewed with appropriate caution.

Resistivity values of the normally well-drained, near-surface deposits in the Lautertal (the water table is normally below the bedrock surface) range from just a few ohm-meters to tens of thousands of ohm-meters (Table A.3). The lowest resistivity values are associated with the fine-grained loam and loess that have retained meteoric water in their pore spaces. The highest resistivity values are associated with competent bedrock. A histogram showing the frequency of resistivity values of the near-surface layers (Figure 13) provided a basis for assigning a range of resistivity values to each of the three near-surface layers commonly observed in the Lautertal. The layer consisting of loam and loess has been assigned a range of resistivity values from 0 to 250 Ω-m; the layer of alluvial and colluvial deposits has been assigned a range of resistivity values from 250 to 800 Ω-m; and bedrock was assigned all resistivity values greater than 800 Ω-m. Choosing the resistivity values separating the three layers was difficult, especially the resistivity value separating the alluvial and colluvial deposits from bedrock.

Locations where loam and loess cover alluvial and colluvial deposits are shown in Figure 14. The resistivity values of the alluvial and colluvial deposits are indicated. This figure corroborates and refines the findings of the electromagnetic data; that is, the alluvium and colluvium appear to be confined to generally north-south- and east-west-trending channels and other depressions in the bedrock surface. The resistivity values of the alluvium and colluvium show no apparent areal trends. This finding is not surprising given the manner in which these sediments were deposited and the possibility that some of the deposits thought to be alluvium and colluvium are, at least in part, fractured and/or dissolved carbonate bedrock. A three-dimensional view of the surface topography and the base of loam and loess is shown in Figure B.3.

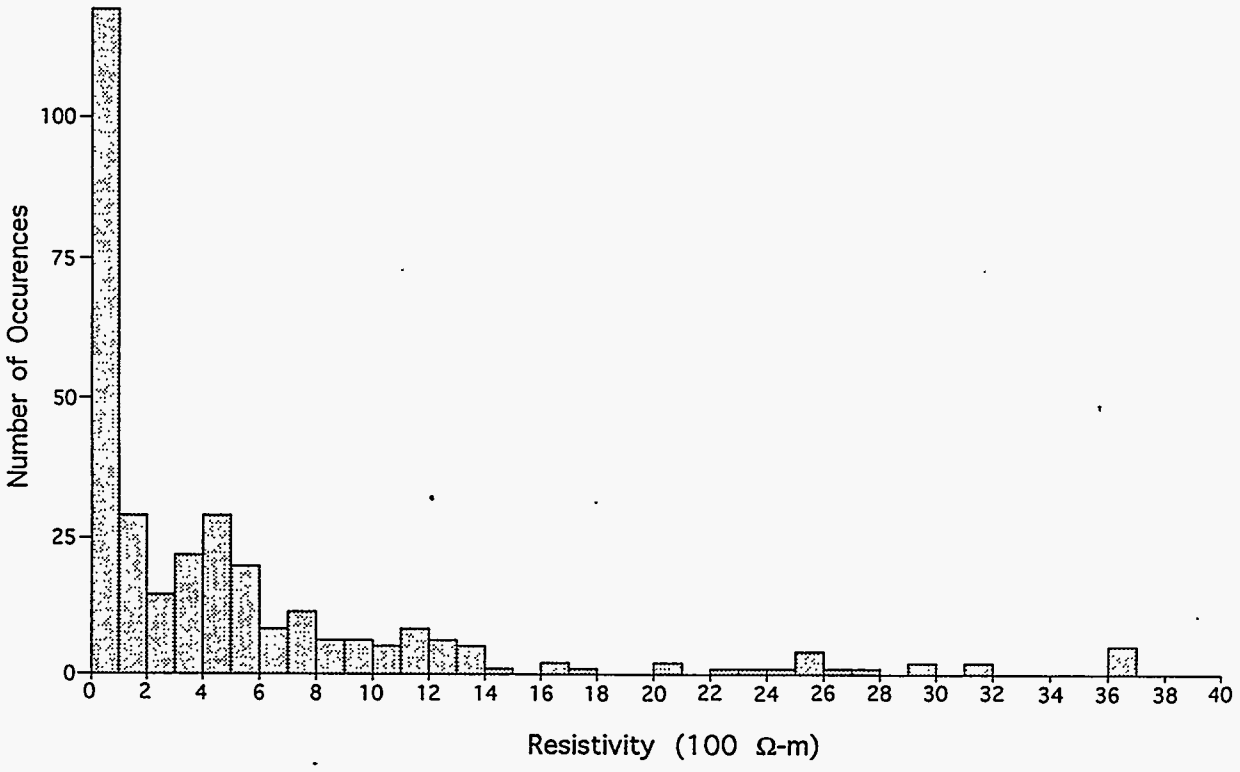

FIGURE 13 Frequency Distribution of the Resistivity of the Near-Surface Layers in the Lautertal Study Area

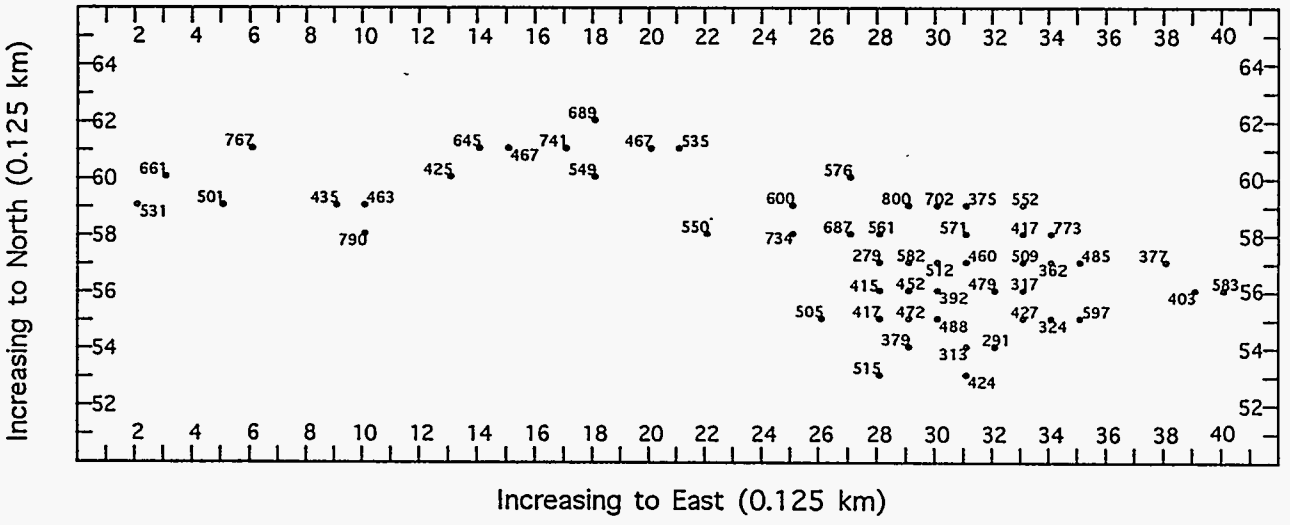

FIGURE 14 Resistivity Distribution Showing Locations Where Loam and Loess Cover Alluvium and Colluvium in the Lautertal Study Area (resistivity values of the alluvial and colluvial deposits are shown in units of ohm-meters)

Locations where the loam and loess lie directly on the bedrock surface are shown in Figure 15. The resistivity values of the bedrock surface are indicated. No areal trends in the resistivity values of the bedrock surface are apparent. (Again, see Figure B.3 for a three-dimensional view of the surface topography and the loam and loess.) If the resistivity values of the bedrock could have been determined at locations in the Lautertal where alluvial and colluvial deposits were present, it might have been possible to discern areal trends related to fracturing and dissolution. As stated previously, coarse alluvial and colluvial deposits can have resistivity values quite similar to those of highly fractured and dissolved carbonate rocks, and, as a result, it is often difficult to separate these two lithotypes on the basis of vertical electrical sounding data.

The layering parameters determined by the inversion of the vertical electrical sounding data have also been used in conjunction with the results of the seismic refraction profiling part of this study to construct maps showing the thickness of the loam and loess, the thickness of the alluvial and colluvial deposits, and the topography of the bedrock surface. The vertical electrical sounding data were considered more reliable in the determination of the thickness of the loam and loess, while the seismic refraction data were considered more reliable in the determination of the thickness of the alluvial and colluvial deposits. Thus, a combination of the results of the vertical electrical soundings and the seismic refraction profiling was used to construct the map showing the topography of the bedrock surface. The loam and loess thickness map is shown in Figure 16. The presentation and discussion of maps showing the thickness of the alluvial and colluvial deposits and the topography of the bedrock surface is deferred to Section 4.4. The thickness of the loam and loess that blanket much of the Lautertal ranges from 0 to approximately 20 m, with the mean value near the middle of that range. The thickness of these fine-grained deposits tends to be greatest above channels and other depressions on the bedrock surface that have not been completely filled with alluvial and colluvial deposits.

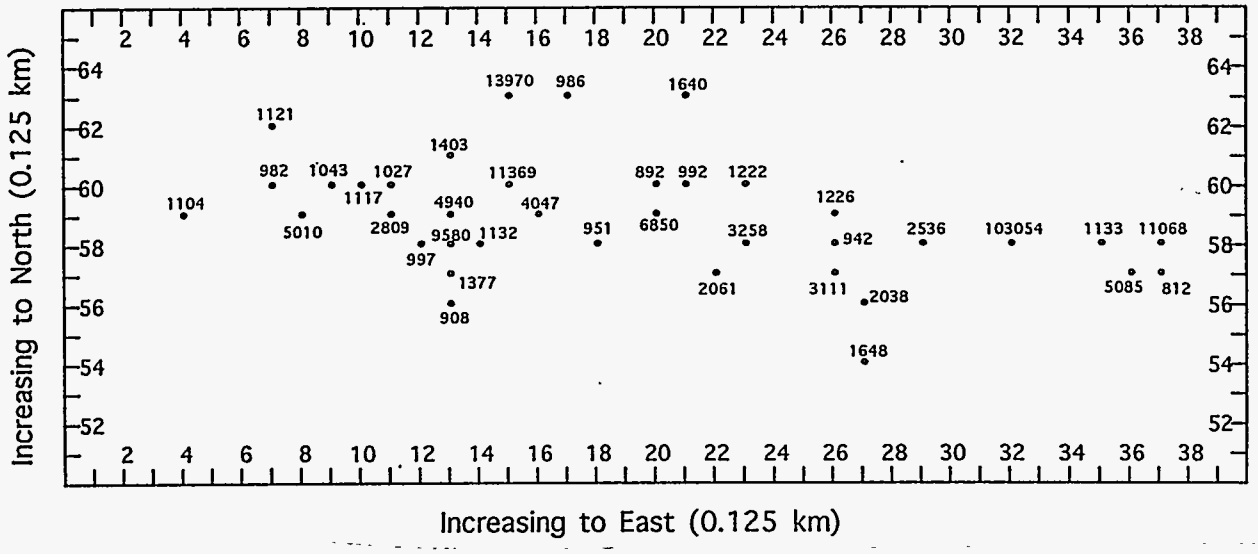

FIGURE 15 Resistivity Distribution Showing Locations Where Loam and Loess Lie Directly on Bedrock Surface in the Lautertal Study Area (resistivity values of the bedrock are shown in units of ohm-meters)

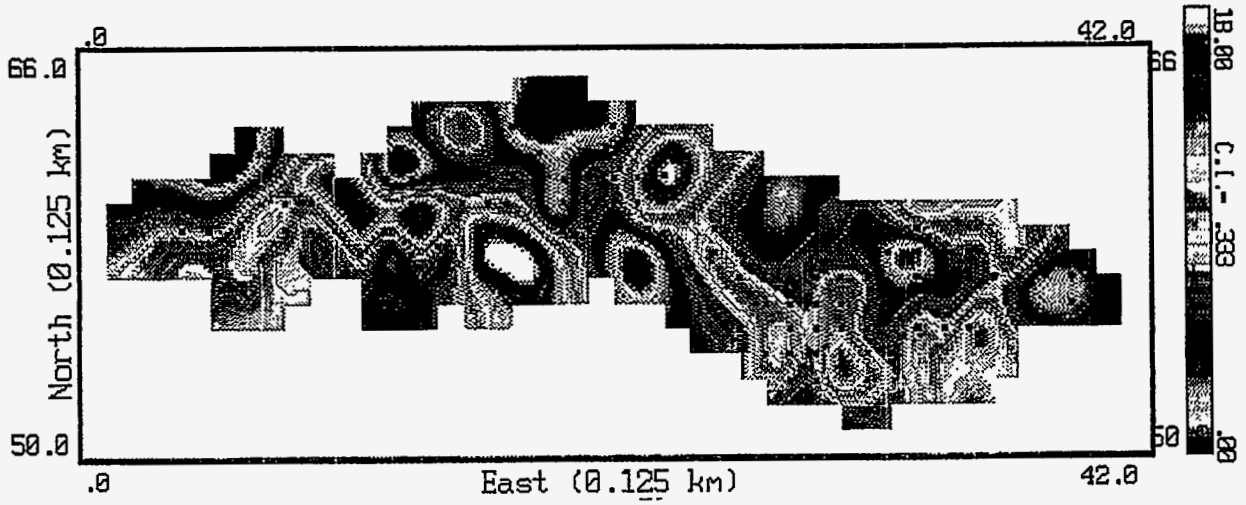

FIGURE 16 Thickness of the Loam and Loess in the Lautertal Study Area

4.4 Seismic Refraction Profiling

Seismic refraction profiling provided another examination of the nature of the near-surface deposits in the Lautertal. This method, perhaps the most definitive of the three employed in this study, involved the use of an energy source to generate seismic waves. Measurements of the travel times of the seismic waves were used to determine the velocity (in meters/second) distribution and the discontinuities of the elastic properties in the near-surface deposits.

Reversed seismic refraction profiles were run at 51 locations throughout the Lautertal. A 12-channel Bison Series 5000 system, along with Geosense 14.5-Hz vertical component geophones, were employed in this phase of the geophysical study. The length of each profile was usually 120 m (10-m geophone spacing). This length was adequate to obtain the depth to the bedrock surface and the velocities of the unconsolidated deposits and the bedrock surface. At some locations, where the unconsolidated deposits resting on the bedrock surface were known to be thin, the length of the profiles was shortened to 60 m (5-m geophone spacing). The source of energy was 0.25 kg of Seismogelit detonated by an instantaneous electrical blasting cap in a hand-augured hole approximately 1.0 m deep.

The locations of the seismic refraction profiles were chosen to optimize the amount of information about the shallow geological framework of the Lautertal in the available time. The information obtained from the seismic refraction profiling should complement the information obtained from the electromagnetic surveying and the vertical electrical soundings. In all but a few cases, the seismic refraction profiles were located on relatively flat terrain, along lines and between nodes of the orthogonal grid covering the Lautertal, to ensure that the geophones were at the same approximate elevation and that the shot-point elevations were known within a meter.

Reduction of the seismic refraction data, a series of time-distance plots, followed a scheme described by Heiland (1968). This scheme assumes that the earth's surface and the interfaces separating layers of rock are planar, at least between the shot points. It also assumes that the velocity of each layer is homogeneous and isotropic between the shot points. If the assumptions of Heiland's scheme are met, points on the time-distance plots will fall on a series of straight lines. Normally, undulations on the earth's surface and/or interfaces and variations in the velocities within the layers cause points on the time-distance plots to deviate from straight lines. In this study, this difficulty was accounted for by fitting least-squares line segments to the appropriate points on the time-distance plots. Results obtained from Heiland's scheme include velocities of the layers, depths to the interfaces below the shot points, and locations of the dips of the interfaces between the shot points (Table A.4).

Reduction of the seismic refraction data was, as previously indicated by the vertical electrical sounding data, a problem involving three layers: (1) loam and loess, (2) alluvial and colluvial deposits, and (3) carbonate bedrock. (Away from the channels and other depressions in the bedrock surface, where the alluvium and colluvium were absent, reduction of the data was a simpler two-layer problem.) A three-dimensional view of the shallow geological framework of the Lautertal, as determined by seismic refraction profiling, is shown in Figure B.4. The three layers had velocities that increased monotonically with depth. The layer of fine-grained loam and loess had a mean velocity of 525 m/s; the layer of alluvium and colluvium had a mean velocity of 1,553 m/s; and the mean velocity of the bedrock surface was 3,721 m/s. The velocity of the bedrock surface had a wide range — from 2,320 to 7,646 m/s. This velocity is characteristic of karstic terrain and highly variable water content. The mean velocities of the two layers of unconsolidated deposits are low, even for the types of deposits comprising these layers. The low values indicate that these deposits were well-drained at the time the seismic refraction profiling was done.

A histogram showing the frequency of the velocities of the near-surface deposits in the Lautertal (Figure 17) clearly indicates the ranges of velocities associated with the three layers. Although the range of velocities associated with the carbonate bedrock is large, it does not appear to overlap the range of velocities associated with the alluvium and colluvium. Thus, velocity is a better parameter than resistivity for differentiating between the alluvial and colluvial deposits and the fractured and/or dissolved bedrock.

Locations where the alluvial and colluvial deposits were encountered during the seismic refraction profiling are shown in Figure 18. The velocity values of these deposits are also shown in this figure. Inspection of the areal distribution of the velocities of the alluvium and colluvium deposits does not indicate any significant trends.

Locations where the seismic refraction profiling was able to determine the depth to bedrock are shown in Figure 19. The velocities of the rocks forming the bedrock surface are also shown in this figure. Visual examination of the areal distribution of the bedrock velocities does not indicate any significant trends. However, these velocities were subjected to statistical analysis in an attempt to determine whether the velocities in the bedrock channels were significantly different

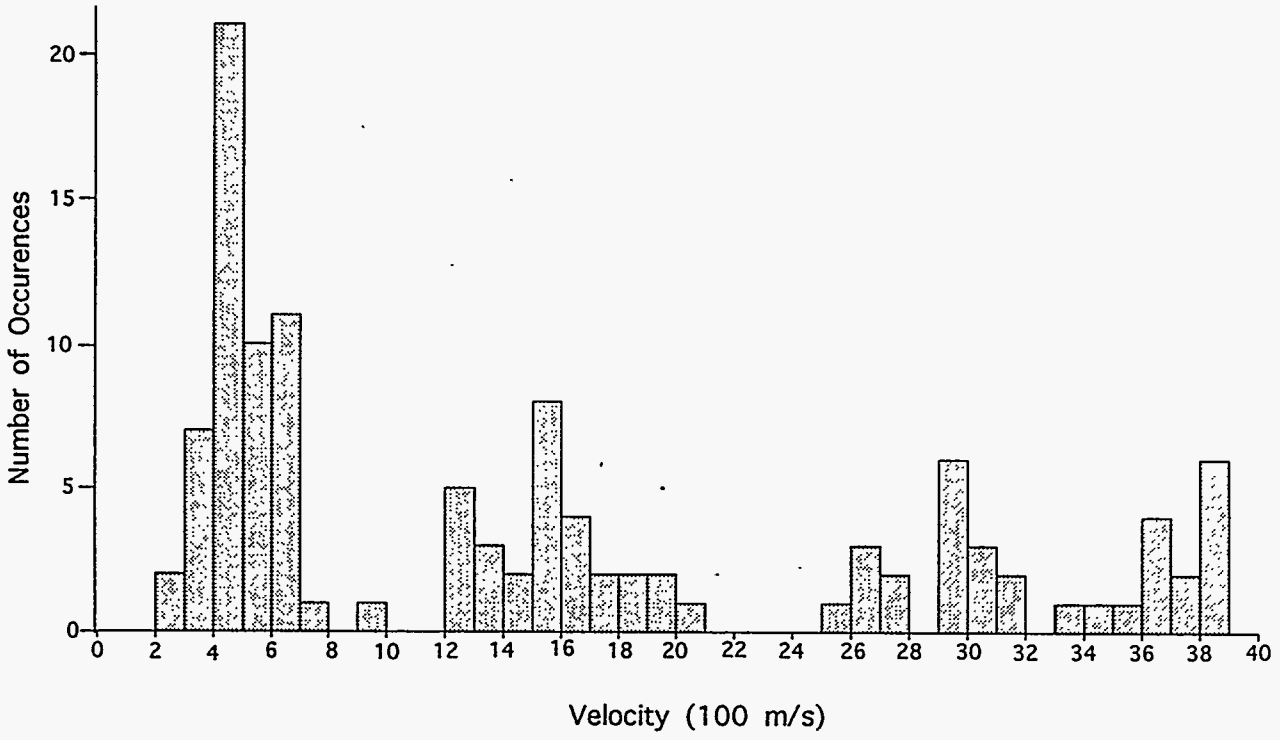

FIGURE 17 Frequency Distribution of the Velocities of the Near-Surface Deposits in the Lautertal Study Area

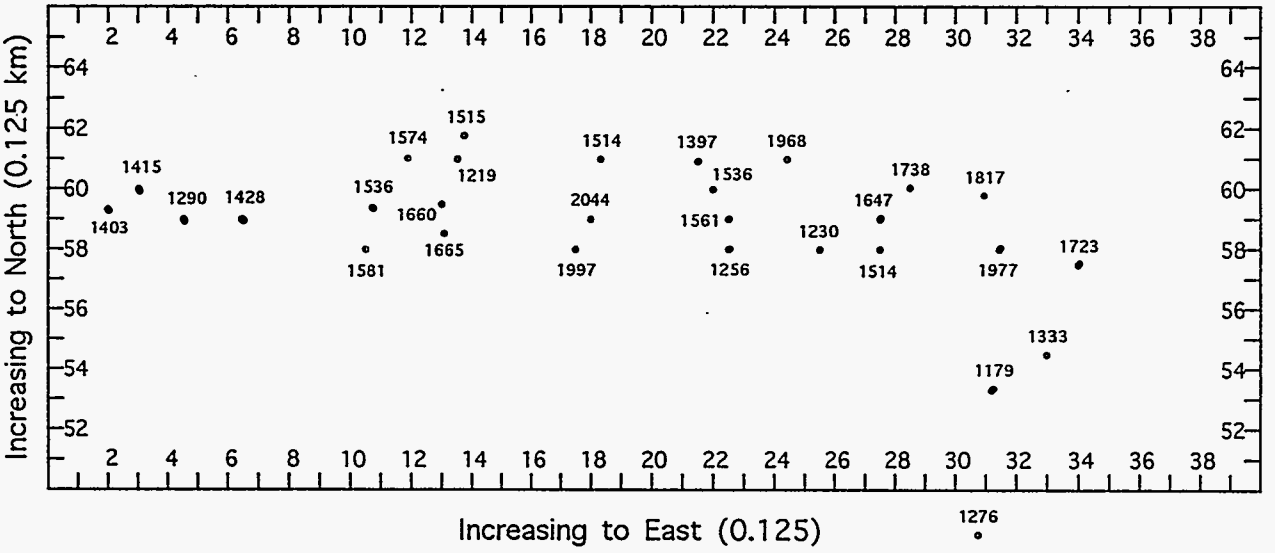

FIGURE 18 Areal Distribution of the Velocities of the Alluvium and Colluvium in the Lautertal Study Area (showing velocity values of the alluvial and colluvial deposits in units of meters per second)

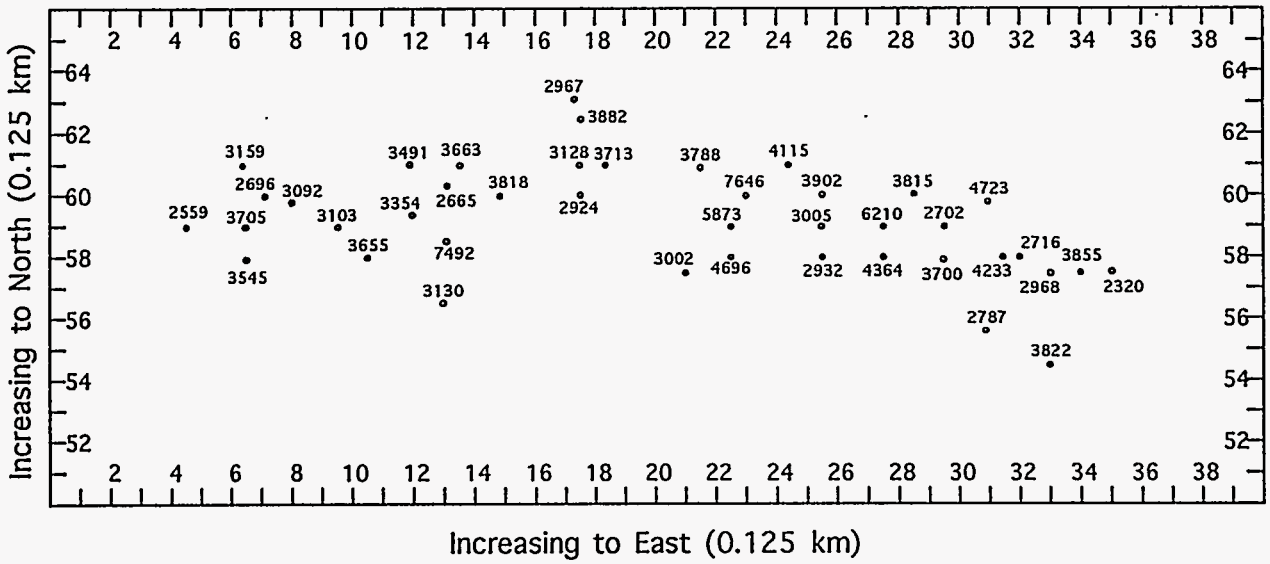

FIGURE 19 Areal Distribution of the Velocities of the Bedrock Surface in the Lautertal Study Area (showing velocities of the bedrock surface in units of meters per second)

from the velocities away from the bedrock channels. The number of bedrock velocity values was limited; therefore, a statistical test was performed in which the hypothesis was stated in terms of population means, and the t-distribution was employed (Lindgren 1960). The sample mean of the bedrock surface velocities in the bedrock channels was 4,247 m/s, whereas the sample mean of the bedrock surface velocities away from the bedrock channels was 3,313 m/s. Results of the statistical test indicate that this difference is significant at the 95% confidence level. The greater mean velocity of the bedrock in the channels is due to the fact that bedrock elevations are lower and the bedrock is saturated. Away from the bedrock channels, the bedrock surface is above the water table. Thus, water content likely plays a greater role than porosity in the determination of the bedrock velocity.

As mentioned previously, results of the seismic refraction profiling were used in conjunction with the results of the vertical electrical soundings to construct maps showing the thickness of the loam and loess, the thickness of the alluvium and colluvium, and the topography of the bedrock surface in the Lautertal. The map showing the thickness of the loam and loess in the Lautertal (Figure 16) was discussed in Section 4.3. The map indicating the thickness of the alluvial and colluvial deposits in the Lautertal is shown in Figure 20. As expected, these deposits were thickest over channels and depressions in the bedrock surface, with the maximum thickness (where measured) in excess of 30 m. The topography of the bedrock surface in the Lautertal is shown in Figure 21. Elevations on the bedrock surface ranged from 385 to 472 m above mean sea level. The lowest elevation on the bedrock surface, as measured by the combination of geophysical methods, is located near the lowest surface elevations in the Lautertal, where surface runoff exits the Lautertal before joining the Lauterach. This low point on the bedrock surface is in the thalweg of the broad, north-south-trending bedrock channel that, as the electromagnetic data suggest, transects the Lautertal on the western side of Wüstung Eggertsheim. A cross section of this north-south-trending bedrock channel is shown in Figure 22. The bedrock surface is quite

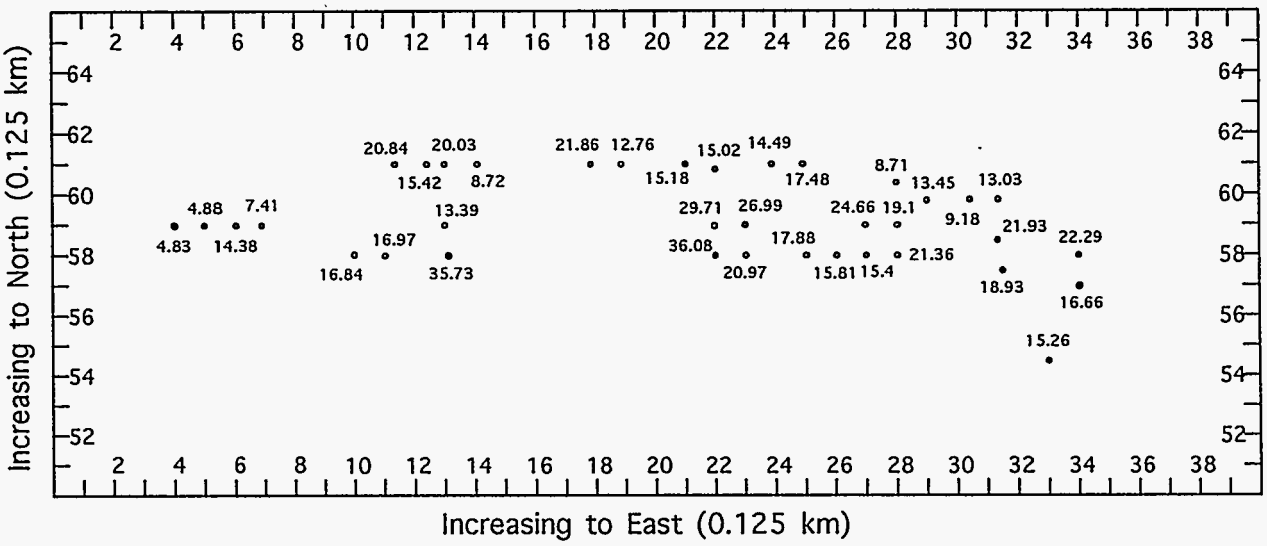

FIGURE 20 Thickness of the Alluvium and Colluvium in the Lautertal Study Area (showing thickness of the alluvial and colluvial deposits in units of meters)

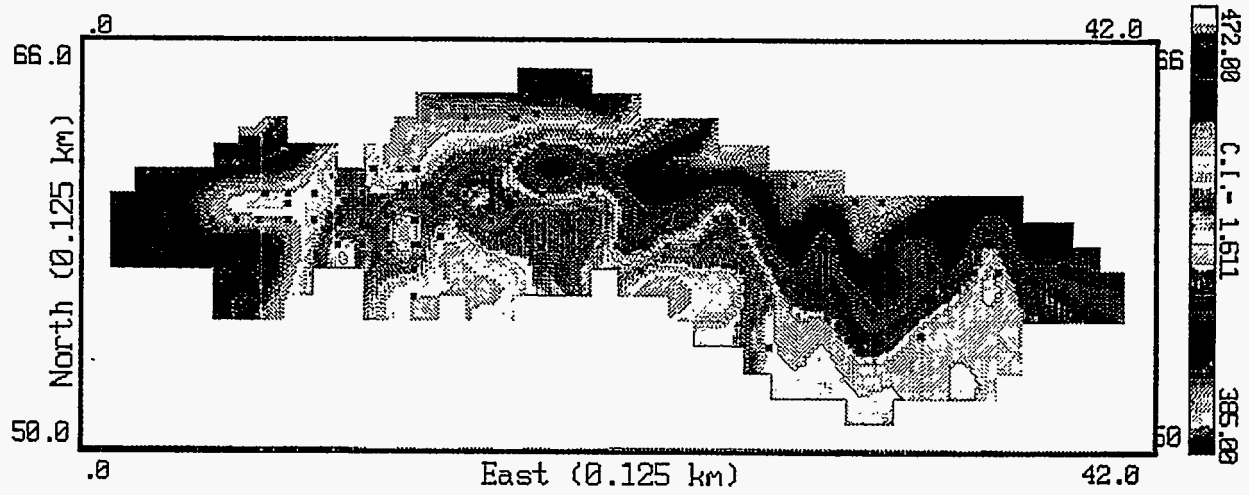

FIGURE 21 Bedrock Topography in the Lautertal Study Area

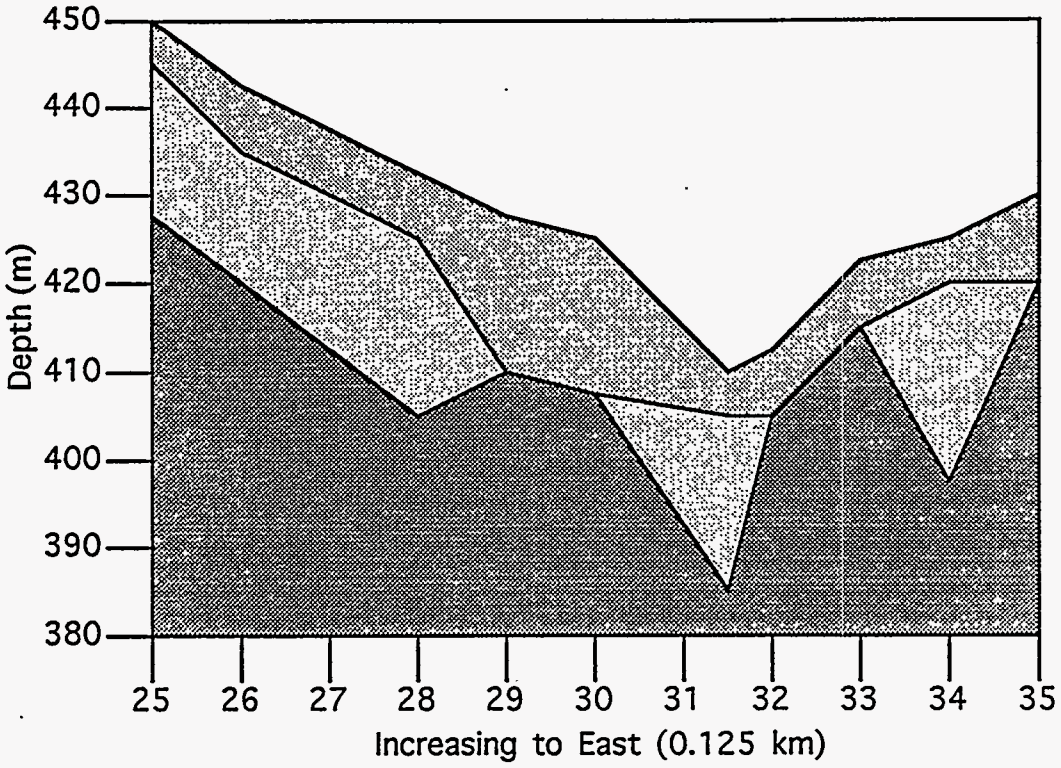

FIGURE 22 Cross Section of the Main North-South-Trending Bedrock Channel in the Lautertal along Line 58 North

irregular, with coarse alluvial and colluvial deposits filling low points on the bedrock surface, whereas the fine-grained loam and loess blanket the entire valley. Note that the loam and loess had thickened over the thalweg before they were eroded by surface drainage. The alluvial and colluvial deposits that continue to the west are associated with an east-west-trending tributary channel. A cross section of that same tributary channel, further to the west in the Lautertal, is shown in Figure 23. Here again the alluvial and colluvial deposits fill the lowest points in the tributary channel before being covered with loam and loess. The highest elevations on the bedrock surface are located in the western and northwestern parts of the Lautertal. At these locations, there are no deep channels or depressions in the bedrock surface and no alluvial and colluvial deposits.

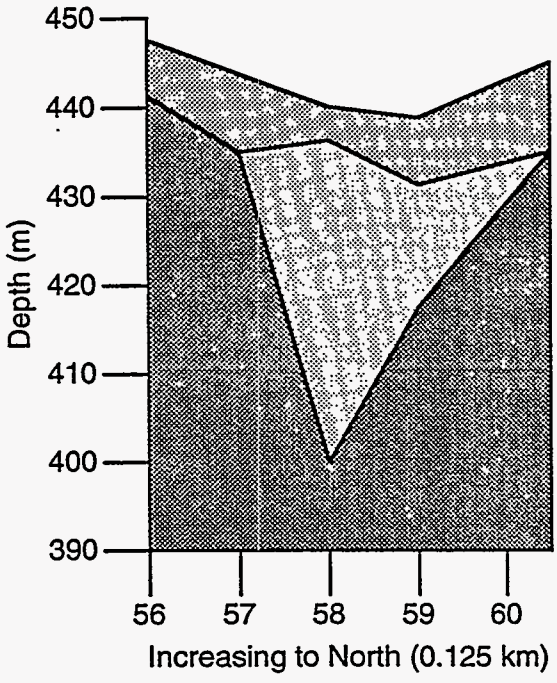

FIGURE 23 Cross Section of the East-West-Trending Bedrock Channel in the Lautertal (tributary to the main bedrock channel) along Line 13 East

5 Discussion

Geophysical exploration was successfully used to determine the shallow geological framework of the Lautertal at the Combat Maneuver Training Center in Hohenfels, Germany. The near-surface deposits in this dry valley, which are typical of the karstic environment of the southern Frankische Alb, consist of three basic layers: (1) a surficial layer of fine-grained loam and loess, (2) a layer of coarse alluvial and colluvial deposits, and (3) a highly fractured and dissolved carbonate bedrock. The layer of fine-grained loam and loess covers most of the Lautertal. The alluvial and colluvial deposits appear to be confined to channels and other depressions in the karstic bedrock surface. The channels and other depressions in the bedrock surface form a trellis-like pattern that is consistent with the preferred directions of fractures and joints in the bedrock. At the time when the geophysical investigations were being conducted in the Lautertal, the two layers of unconsolidated deposits appeared to be well-drained.

All of the geophysical methods employed in this study — electromagnetic surveying, vertical electrical soundings, and seismic refraction profiling — made significant contributions to the understanding of the shallow geological framework of the Lautertal. Even though the individual methods had shortcomings, the three methods complemented each other well. They should be included in similar future exploration programs.

The electromagnetic surveying provided a qualitative view of the electrical properties of the near-surface deposits. In this method, electrical conductivity is the parameter that is related to lithology. From the findings of this surveying, the locations and shapes of channels and other depressions in the low-conductivity carbonate bedrock surface were determined, and the higher-conductivity unconsolidated deposits resting on the bedrock surface were separated into two layers: (1) a layer of less-conductive, coarse deposits (alluvium and colluvium) confined to bedrock channels and depressions and (2) a layer of more-conductive fine-grained deposits (loam and loess).

The vertical electrical soundings provided a quantitative view of the electrical properties of the near-surface deposits. Layering parameters (resistivities and thicknesses), obtained by inverting data gathered in the field, confirmed and refined the results of the electromagnetic surveying. There were, however, disappointments associated with the vertical electrical soundings. The lack of resistivity contrast between the well-drained, coarse alluvial and colluvial deposits and the highly fractured and dissolved bedrock surface precludes locating the interface of these two layers with any confidence.

Seismic refraction data were readily inverted to layering parameters (velocities and thicknesses) by employing classical seismic refraction theory. The seismic velocities of the near-surface deposits increased monotonically with depth, and there were always sizable velocity contrasts at the interfaces separating the near-surface layers, even at locations where alluvial and colluvial deposits rested on a highly fractured and dissolved bedrock surface. The only difficulty encountered in the seismic refraction profiling came as the result of having to detonate the energy

source in the surficial, fine-grained loam and loess. These deposits appreciably damped the seismic energy.

All phases of this geophysical study — acquisition, processing, and interpretation — were quite satisfactory. However, the entire process could have been improved with downhole geological and geophysical control. Detailed samples and full suites of downhole geophysical logs from strategically located test borings, planned for later in this hydrogeological study, will allow reexamination and refinement of interpretation obtained from all geophysical data gathered to date.

Several important aspects of the hydrogeology of the Lautertal region have become clear on the basis of observations made during the course of this study. Groundwater recharge in the Lautertal is impeded by the widespread surficial layer of fine-grained loam and loess. This layer has a mean thickness of approximately 10 m, and published hydraulic conductivity values for these types of materials are in the 10^{-5} to 10^{-9} m/s range (Todd 1964). Given the considerable clay content of these deposits, their hydraulic conductivities likely fall near the low end of this range. In any event, infiltration of meteoric waters through these deposits appears to occur at a very low rate. Much of the meteoric water that falls directly on the Lautertal leaves as runoff. There are isolated places in the Lautertal where the layer of fine-grained loam and loess is not present. In those places, the coarse alluvial and colluvial deposits that fill the channels and other depressions in the bedrock surface are exposed.

The geologic map of the Velburg quadrangle (Meyer 1990) shows that the fluvial deposits known as the Schutzfelsschicten (Upper Cretaceous) are exposed in the western portion of the Lautertal. These deposits and the Pleistocene and Recent alluvial and colluvial deposits that occupy the channels and other depressions in the bedrock surface likely have hydraulic conductivities considerably higher than the loam and loess. As a result, these coarse deposits allow meteoric waters better access to the fractured and dissolved bedrock aquifers below. However, the rather small exposure of the coarse deposits probably limits the intake of meteoric waters.

The best access that the meteoric waters have to the main shallow bedrock aquifer in the Malm Formation appears to be through the exposed bedrock in the uplands away from the valleys. Some of the exposed bedrock in the uplands belongs to the Upper Kimmeridge (Epsilon) Member of the Malm Formation. This resistant rock caps the higher knolls in this region and does not have a fracture and dissolution porosity as great as the older rocks of the Middle Kimmeridge (Delta) Member of the Malm Formation, which are exposed closer to but still in the uplands away from the dry valleys. In the Lautertal region, rocks of the Middle Kimmeridge Member form more of the earth's surface than any other geological unit. These rocks also form the bedrock surface under many of the dry valleys like the Lautertal. If the rocks of the Middle Kimmeridge Member of the Malm Formation allow meteoric waters almost direct and unimpeded pathways to the main Malm aquifer, a hydraulic scenario is possible that would explain the turbid discharges observed in some of the perennial streams during and shortly after heavy rainfall.

6 Conclusions and Recommendations

A geophysical study in the Lautertal at the Combat Maneuver Training Center in Hohenfels, Germany, was conducted to determine the shallow geological framework of a typical dry valley in the karstic environment of the southern Frankische Alb and, thereby, to gain insights into the role that the dry valleys in the region play in the shallow groundwater flow system. Not only was this goal achieved, but other areas were indicated where additional research is necessary to understand the total groundwater flow system.

The most significant conclusions of this study are as follows:

- A combination of carefully selected geophysical methods was successfully used to determine the shallow geological framework of a typical dry valley in this complex karstic environment.

- In dry valleys like the Lautertal, infiltration of meteoric waters into the subsurface is generally impeded by a surficial layer of fine-grained, low-hydraulic-conductivity loam and loess.

- Most groundwater recharge occurs in the uplands where the Middle Kimmeridge (Delta) Member of the Malm Formation (Jurassic) is widely exposed. These carbonate rocks are known to be susceptible to dissolution along structurally induced fractures and joints; thus, they offer ready access to the main shallow aquifers lower in the Malm Formation.

- The carbonate rocks of the Middle Kimmeridge Member of the Malm Formation appear to be closely associated with the localized occurrence of increased turbidity in perennial streams (such as the Lauterach) during or shortly after heavy rainfall.

On the basis of these conclusions, it is recommended that future efforts to understand the total shallow groundwater flow system of the Hohenfels region be focused on those areas where the bulk of groundwater recharge takes place, i.e., the uplands and the valley side slopes. The primary target of this research should be the Middle Kimmeridge Member of the Malm Formation.

Specific recommendations for future research are as follows:

- Detailed fracture pattern analysis of the carbonate rocks in the uplands should be given highest priority. Aerial photos, cave and spring inventories, and identification of catchments are all important. Ground and/or airborne time-domain electromagnetic surveying may prove useful in identifying fracture density and orientation in the subsurface.

- Water wells within a specified distance of the Combat Maneuver Training Center should be inventoried. Knowledge of water levels, water chemistry, and the results from pump tests would be very useful in quantifying localized flow system parameters.

- Pertinent meteorological data should be gathered. Precipitation, evapotranspiration, and barometric pressure data have relevance to water budgets and the observed occurrences of turbidity in such perennial streams as the Lauterach.

- Chemical analysis of the waters of the Lauterach where turbidity has occurred should provide information on the source of groundwater inflow.

- High resolution surficial geophysical exploration data (ground-penetrating-radar and seismic-velocity profiling) should be collected near the point in the Lauterach where turbidity has occurred. Fractures and solution cavities in the upper bedrock should be targeted.

7 References

Andres, G., and H. Wirth, 1985, Grundwassergleichenkarte von Bayern (1:500000), Bayerisches Landesamt für Wasserwirtschaft.

Apel, R., 1971, "Hydrogeologische Untersuchungen im Malmkarst der Südlichen und Mittleren Frankenalb," *Geologica Bavarica* 64:268-355, München.

Bayerisches Geologisches Landesamt, 1981, Geologische Karte von Bayern (1:500000), München, Germany.

Bayerisches Landesamt für Wasserwirtschaft, 1987, Die Grundwasserneufildung in Bayern Informationsberichte ISSN 0176-4217.

Dobrin, M.B., and C.H. Savit, 1988, *Introduction to Geophysical Prospecting,* McGraw-Hill Book Company, New York, N.Y.

Ebasco-Dorsch Consultants, Inc., 1990, *Sanitary Landfill Investigations at Hohenfels Training Area,* report prepared for the U.S. Army Engineer Division, Europe, CEEUD-ED-MC, Contract No. DACA 90-88-D-0058.

Freyberg, B.V., 1969, "Tektonische Karte der Frankischen Alb und ihrer Umgebung Erlanger," *Geologische Abhandlungen* 77, Erlangen.

Fuhrmann, D., 1977, Stratigraphische und Tektonische Untersuchungen auf der Kartenblättern Kastl und Velburg (1:25000), Dipl. Arb., University of Erlangen, Erlangen.

Heiland, C.A., 1968, *Geophysical Exploration,* Hafner Publishing Co., New York, N.Y.

Interpex Limited, 1988, *Resix Plus User's Manual,* Golden, Colo.

Lattman, L.A., and R.R. Parizek, 1964, "Relationship between Fracture Traces and the Occurrences of Groundwater in Carbonate Rocks," *Journal of Hydrology* 2:73-91.

Lindgren, B.W., 1960, *Statistical Theory,* MacMillan Company, New York, N.Y.

Meyer, R.F.K., 1990, Erlauterungen zur Geologische, Karte Blatt. Nr. 6736 Velburg (1:25000), Bayerisches Geologishes Landesamt, München, Germany.

Schoger, H., 1992, *Study of the Old Landfill, Hohenfels, Phase I,* Wolf-Blumenthal Ingenieurbüro, Nürnberg, Germany, report prepared for Combat Maneuver Training Center, Hohenfels, Germany, Contract No. DACA 90-90-D-0053.

Telford, W.M., L.P. Geldart, R.E. Sheriff, and D.A. Keys, 1976, *Applied Geophysics,* Cambridge University Press, New York, N.Y.

Todd, D. K., 1964, *Groundwater Hydrology,* John Wiley and Sons, Inc., New York, N.Y.

Appendix A:

Data for the Geophysical Studies in the Lautertal

TABLE A.1 Surface Elevations in the Lautertal Study Area

Nodal Coordinates	Surface Elevations (meters above msl[a])
02 58	479.8
02 59	483.1
03 58	481.9
03 59	467.8
03 60	474.6
04 58	479.2
04 59	462.6
04 60	466.8
05 58	471.2
05 59	459.0
05 60	459.2
06 56	483.0
06 57	476.7
06 58	462.5
06 59	455.9
06 60	455.8
06 61	466.0
07 56	476.9
07 57	469.6
07 58	460.9
07 59	452.8
07 60	451.8
07 61	461.1
07 62	471.0
08 57	462.7
08 58	457.0
08 59	451.3
08 60	449.7
08 61	462.3
09 58	454.9
09 59	451.9
09 60	448.2
09 61	467.0
10 58	448.4
10 59	450.4
10 60	448.8
11 58	444.2
11 59	447.7
11 60	448.8
12 56	460.0
12 57	450.7
12 58	442.4
12 59	441.8
12 60	447.9
12 61	464.9
13 56	447.3
13 57	443.3
13 58	440.4
13 59	439.0
13 60	441.4
13 61	456.7
13 62	470.5
14 57	454.3
14 58	450.1
14 59	441.7
14 60	440.6
14 61	449.8
14 62	459.0
14 63	458.4
15 57	476.0
15 58	460.0
15 59	447.3
15 60	435.1
15 61	441.7
15 62	448.8
15 63	454.5
16 56	485.1
16 57	473.4
16 58	462.5
16 59	448.2
16 60	436.2
16 61	435.8
16 62	442.9
16 63	454.6
17 57	471.7
17 58	459.5
17 59	448.7
17 60	437.2
17 61	432.2
17 62	443.5
17 63	456.9

TABLE A.1 Cont.

Nodal Coordinates	Surface Elevations (meters above msl[a])
18 57	461.8
18 58	453.0
18 59	444.5
18 60	435.3
18 61	430.3
18 62	440.8
18 63	454.8
18 64	479.3
19 57	454.9
19 58	n.m.[b]
19 59	443.3
19 60	435.4
19 61	428.7
19 62	438.4
19 63	451.6
19 64	467.9
20 58	n.m.
20 59	440.3
20 60	436.8
20 61	428.0
20 62	439.3
20 63	453.4
21 58	435.3
21 59	431.3
21 60	429.7
21 61	426.2
21 62	438.5
21 63	454.7
22 57	452.8
22 58	449.2
22 59	440.6
22 60	426.6
22 61	425.0
22 62	437.6
23 57	460.2
23 58	451.4
23 59	440.9
23 60	426.9
23 61	423.5
23 62	435.3
24 56	467.4
24 57	463.5
24 58	453.6
24 59	441.0
24 60	431.0
24 61	420.8
24 62	432.9
25 55	462.8
25 56	452.9
25 57	461.9
25 58	450.4
25 59	437.8
25 60	429.7
25 61	419.1
26 55	445.7
26 56	442.9
26 57	453.5
26 58	443.5
26 59	434.8
26 60	428.1
26 61	418.3
27 54	440.2
27 55	439.3
27 56	435.1
27 57	441.6
27 58	437.4
27 59	430.7
27 60	422.2
28 53	436.9
28 54	434.9
28 55	437.8
28 56	432.2
28 57	433.4
28 58	432.4
28 59	425.0
28 60	415.8
29 53	431.5
29 54	430.5
29 55	434.8
29 56	430.1
29 57	430.1
29 58	429.2
29 59	421.0
29 60	411.0

TABLE A.1 Cont.

Nodal Coordinates	Surface Elevations (meters above msl[a])
30 53	431.0
30 54	425.5
30 55	429.6
30 56	426.1
30 57	422.3
30 58	426.9
30 59	419.0
31 52	429.4
31 53	426.7
31 54	428.6
31 55	419.3
31 56	423.0
31 57	419.5
31 58	417.9
31 59	416.4
32 54	423.7
32 55	432.3
32 56	431.0
32 57	420.7
32 58	411.1
32 59	403.6
33 53	442.0
33 54	431.0
33 55	428.8
33 56	433.2
33 57	425.4
33 58	422.8
33 59	415.7
34 53	447.7
34 54	437.5
34 55	432.1
34 56	438.5
34 57	430.4
34 58	425.1
35 53	449.9
35 54	438.6
35 55	442.2
35 56	444.1
35 57	435.2
35 58	429.2
35 59	435.9
36 54	452.6
36 55	n.m.
36 56	454.2
36 57	437.3
36 58	437.8
36 59	438.7
37 56	452.3
37 57	442.8
37 58	443.2
38 56	452.7
38 57	447.9
38 58	442.4
39 56	454.9
39 57	449.6
40 56	458.7

[a] msl = mean sea level.

[b] n.m. = no measurement.

TABLE A.2 Electromagnetic Surveying Data

Nodal Coordinates	Apparent Conductivity at Transmitter-Receiver Separation (mmho/m)		
	10 m	20 m	40 m
02 58	7.1	5.5	1.9
02 59	6.8	5.4	2.1
03 58	3.9	4.4	1.3
03 59	11.5	10.5	5.7
03 60	12.0	8.5	5.5
04 58	9.3	9.2	8.2
04 59	14.0	12.0	7.2
04 60	2.7	2.65	1.1
05 58	7.1	5.5	1.9
05 59	12.0	9.4	2.9
05 60	3.9	4.0	1.6
06 56	8.8	7.7	3.4
06 57	6.0	5.8	1.5
06 58	11.0	6.2	2.0
06 59	6.6	4.3	0.3
06 60	7.4	4.8	2.0
06 61	1.4	1.0	0.1
07 56	6.8	5.9	3.4
07 57	1.4	1.5	0.2
07 58	6.3	3.4	0.4
07 59	2.5	1.7	0.6
07 60	6.65	4.6	0.9
07 61	1.8	1.2	0.5
07 62	7.1	4.9	1.8
08 57	11.0	9.0	3.5
08 58	18.0	14.5	5.5
08 59	10.0	8.0	3.0
08 60	14.5	11.5	0.5
08 61	1.4	1.4	0.9
09 58	17.5	14.0	8.5
09 59	12.5	12.0	5.9
09 60	15.0	12.0	5.25
09 61	1.2	0.9	0.6
10 58	15.5	12.5	6.0
10 59	16.0	13.0	6.8
10 60	11.2	6.5	2.9

TABLE A.2 Cont.

Nodal Coordinates	Apparent Conductivity at Transmitter-Receiver Separation (mmho/m) 10 m	20 m	40 m
11 58	14.0	11.5	6.0
11 59	11.5	10.0	4.4
11 60	4.9	5.1	4.2
12 56	8.5	7.0	4.0
12 57	5.8	5.3	2.0
12 58	12.0	9.0	3.5
12 59	11.0	7.0	1.0
12 60	5.1	3.8	1.2
12 61	1.0	0.9	1.0
13 56	9.5	7.0	2.5
13 57	17.0	15.0	7.0
13 58	5.6	4.2	4.1
13 59	25.0	19.0	12.0
13 60	5.0	4.3	3.2
13 61	10.5	6.5	5.0
13 62	2.1	1.8	0.8
14 57	1.8	2.0	0.8
14 58	0.9	1.5	1.2
14 59	3.4	3.0	3.0
14 60	2.6	2.9	1.2
14 61	4.5	3.5	1.5
14 62	5.0	3.5	1.5
14 63	9.0	7.5	3.5
15 57	2.0	1.5	0.1
15 58	1.5	1.5	0.5
15 59	2.0	2.5	1.0
15 60	17.5	13.5	6.0
15 61	3.0	4.0	0.5
15 62	12.0	9.5	5.0
15 63	25.0	19.0	9.0
16 56	1.0	1.0	0.6
16 57	1.5	1.0	2.5
16 58	1.5	1.0	1.0
16 59	4.5	4.0	2.5
16 60	5.5	5.0	3.0
16 61	8.0	7.5	5.0
16 62	15.0	13.0	3.5
17 57	4.0	4.0	1.5
17 58	2.5	2.5	1.5
17 59	2.5	2.5	2.0

TABLE A.2 Cont.

Nodal Coordinates	Apparent Conductivity at Transmitter-Receiver Separation (mmho/m)		
	10 m	20 m	40 m
17 60	3.5	4.0	3.0
17 61	14.0	12.5	7.0
17 62	3.0	2.5	1.0
17 63	3.0	2.0	2.0
18 57	7.0	6.5	4.5
18 58	10.5	8.0	6.0
18 59	5.0	6.0	5.0
18 60	18.0	15.5	5.0
18 61	18.0	14.5	6.0
18 62	6.0	4.5	1.0
18 63	5.0	4.0	2.0
18 64	2.0	1.5	1.0
19 57	15.0	14.5	6.0
19 58	16.5	12.0	9.0
19 59	9.0	8.0	4.5
19 60	14.5	10.5	7.0
19 61	13.5	12.0	8.5
19 62	3.5	2.25	1.5
19 63	3.0	2.0	1.0
19 64	2.0	1.5	1.5
20 59	18.0	12.0	9.0
20 60	12.0	9.0	1.0
20 61	11.0	8.5	5.0
20 62	4.0	3.0	2.0
20 63	2.0	1.5	1.5
21 58	7.25	7.0	3.5
21 59	9.0	8.0	7.0
21 60	17.0	11.0	7.0
21 61	10.5	7.5	3.5
21 62	3.0	2.5	1.0
21 63	5.0	4.0	2.0
22 57	4.0	3.0	1.0
22 58	3.0	2.5	1.0
22 59	3.8	2.6	1.1
22 60	7.5	7.5	8.0
22 61	12.0	11.0	6.5
22 62	1.4	1.4	1.4
23 57	2.0	2.0	1.5
23 58	5.5	3.0	4.0
23 59	5.0	4.5	4.5

TABLE A.2 Cont.

Nodal Coordinates	Apparent Conductivity at Transmitter-Receiver Separation (mmho/m) 10 m	20 m	40 m
23 60	17.5	15.0	9.5
23 61	11.0	9.5	7.0
23 62	3.9	3.0	1.5
24 56	1.6	1.4	1.2
24 57	4.5	4.3	0.4
24 58	1.3	1.4	0.3
24 59	5.1	4.1	1.6
24 60	3.0	3.5	2.5
24 61	13.0	11.5	7.0
24 62	2.8	2.8	1.9
25 55	2.1	2.5	2.6
25 56	2.9	3.3	1.6
25 57	8.0	5.0	0.3
25 58	5.5	6.2	2.0
25 59	4.3	3.5	0.5
25 60	2.5	3.2	1.4
25 61	12.0	11.5	5.0
26 55	7.4	5.6	2.5
26 56	13.5	10.5	5.0
26 57	11.0	6.0	1.5
26 58	15.5	11.0	7.0
26 59	18.0	13.5	5.0
26 60	7.0	6.0	1.5
26 61	13.0	10.0	6.0
27 54	24.0	20.0	8.0
27 55	12.0	9.0	4.0
27 56	23.0	18.0	9.0
27 57	17.0	14.5	8.5
27 58	18.0	13.5	7.0
27 59	7.0	3.0	1.5
27 60	18.0	14.0	9.5
28 53	22.0	13.5	8.0
28 54	19.5	17.0	11.0
28 55	18.0	17.0	9.0
28 56	20.0	16.5	
28 57	18.0	13.5	7.0
28 58	22.0	17.0	10.0
28 59	18.0	14.0	8.0
28 60	9.5	9.0	4.0

TABLE A.2 Cont.

Nodal Coordinates	Apparent Conductivity at Transmitter-Receiver Separation (mmho/m)		
	10 m	20 m	40 m
29 53	16.0	15.0	11.5
29 54	21.0	18.0	10.0
29 55	22.0	17.5	9.0
29 56	18.0	15.0	7.0
29 57	26.0	23.0	13.0
29 58	29.0	25.0	16.0
29 59	18.0	13.0	8.0
30 53	16.0	18.0	11.0
30 54	19.5	18.0	11.0
30 55	16.5	14.0	8.0
30 56	6.5	4.5	4.0
30 57	11.0	9.5	6.0
30 58	19.0	16.5	11.0
30 59	11.0	9.0	6.0
31 52	18.0	15.0	7.0
31 53	11.0	10.0	7.5
31 54	12.0	8.5	7.0
31 55	13.0	9.0	7.0
31 56	3.0	4.0	2.5
31 57	6.0	5.0	2.0
31 58	10.0	9.0	5.0
31 59	5.0	5.0	3.0
32 54	12.5	10.0	6.5
32 55	4.5	3.5	3.0
32 56	7.0	5.5	3.5
32 57	3.5	3.5	2.5
32 58	12.5	8.0	4.5
32 59	6.0	5.0	4.0
33 53	7.5	6.0	1.5
33 54	11.5	9.0	6.0
33 55	11.5	9.0	6.5
33 56	8.0	7.5	3.0
33 57	18.0	14.0	7.5
33 58	3.5	4.5	2.0
33 59	4.0	3.8	4.0
34 53	8.5	6.0	2.0
34 54	7.5	5.5	3.5
34 55	23.0	20.5	12.5
34 56	10.0	8.5	4.5
34 57	11.5	8.0	4.5

TABLE A.2 Cont.

Nodal Coordinates	Apparent Conductivity at Transmitter-Receiver Separation (mmho/m)		
	10 m	20 m	40 m
34 58	7.0	8.0	3.5
35 53	7.5	6.5	2.0
35 54	9.0	8.0	3.0
35 55	8.5	8.0	4.0
35 56	4.0	4.0	3.5
35 57	12.0	8.0	5.0
35 58	16.6	13.5	7.0
35 59	8.0	7.0	4.0
36 56	1.8	2.6	1.5
36 57	14.5	11.0	6.0
36 58	6.0	7.0	4.5
36 59	7.0	8.0	4.0
37 56	12.0	6.0	3.5
37 57	7.5	6.0	4.5
37 58	6.5	7.0	3.0
38 56	7.0	5.5	2.5
38 57	22.0		
38 58	17.0	14.5	9.0
39 56	12.5	13.0	4.5
39 57	13.0	11.0	5.0
40 56	12.0	8.0	4.0

TABLE A.3 Results of Inversion of Vertical Electrical Sounding Data

Nodal Coordinates	Surface Elevation (meters above msl[a])	Layer Resistivity (Ω-m)	Layer Thickness (m)
02 59	483.1	93	6.47
		531	
03 60	474.6	60	4.78
		661	
04 59	462.6	51	9.91
		1104	
05 59	459.0	57	5.94
		501	
05 60	459.2	129	2.49
		252	15.51
		985	
06 59	455.9	48	4.11
		119	7.24
		7367	
06 60	455.8	13	0.72
		4209	0.58
		74	7.85
		14,820	
06 61	466.0	474	5.34
		767	
07 59	452.8	1365	0.90
		426	37.22
		1125	
07 60	451.8	121	10.34
		982	
07 61	461.1	2593	2.06
		171	3.17
		1231	
07 62	471.0	19	0.72
		1121	
08 59	451.3	66	11.21
		5010	
08 60	449.7	30	2.25
		113	10.60
		1440	

TABLE A.3 Cont.

Nodal Coordinates	Surface Elevation (meters above msl[a])	Layer Resistivity (Ω-m)	Layer Thickness (m)
08 61	462.3	831	3.55
		3172	4.01
		781	
09 59	451.9	47	5.96
		435	
09 60	448.2	50	8.92
		1043	
10 58	448.4	38	6.13
		790	
10 59	450.4	32	3.50
		463	
10 60	448.8	127	19.48
		1117	
11 58	444.2	49	6.58
		150	3.37
		1246	
11 59	447.2	4	0.90
		2809	
11 60	448.8	179	23.98
		1027	
12 58	442.4	5	1.46
		997	
12 59	441.8	29	3.38
		1880	1.86
		32	8.21
		61,560	
12 60	447.9	369	8.25
		589	7.42
		373	
12 61	464.9	575	8.72
		2283	15.74
		591	
13 56	447.3	71	3.54
		908	
13 57	443.3	43	8.25
		1377	

TABLE A.3 Cont.

Nodal Coordinates	Surface Elevation (meters above msl[a])	Layer Resistivity (Ω-m)	Layer Thickness (m)
13 58	440.4	91	11.22
		9580	
13 59	439.0	30	14.31
		4940	
13 60	441.4	134	18.98
		425	
13 61	456.7	33	1.59
		1403	
14 58	450.1	153	1.32
		1132	
14 59	441.7	154	1.11
		2957	2.73
		50	8.21
		5374	
14 60	440.6	98	1.26
		4205	2.83
		40	7.03
		1769	
14 61	449.8	94	2.52
		645	
15 59	447.3	812	5.05
		278	12.30
		809	
15 60	435.1	39	10.52
		11,369	
15 61	441.7	467	
15 62	448.8	43	2.40
		77	18.18
		34,080	
15 63	454.5	21	8.12
		13,970	
16 59	448.2	229	22.84
		4047	

TABLE A.3 Cont.

Nodal Coordinates	Surface Elevation (meters above msl[a])	Layer Resistivity (Ω-m)	Layer Thickness (m)
16 60	436.2	30	1.46
		363	67.64
		10,500	
16 61	435.8	86	4.23
		271	61.67
		10,580	
17 57	471.7	242	5.29
		2388	15.81
		100	
17 59	448.7	684	13.32
		145	8.40
		1300	
17 60	437.2	247	4.28
		555	13.69
		143	28.24
		8025	
17 61	432.2	46	7.03
		741	
17 62	443.5	183	0.67
		981	9.71
		347	34.27
		725	
17 63	456.9	416	10.45
		986	
18 58	453.0	134	16.30
		951	
18 60	435.3	29	5.04
		549	
18 61	430.3	30	5.67
		418	17.16
		1912	
18 62	440.8	54	1.05
		689	
19 59	443.3	49	2.65
		192	19.76
		423	

TABLE A.3 Cont.

Nodal Coordinates	Surface Elevation (meters above msl[a])	Layer Resistivity (Ω-m)	Layer Thickness (m)
19 60	435.4	22	1.25
		156	20.81
		1102	
19 61	428.7	21	1.33
		306	43.06
		1181	
19 62	438.4	100	1.17
		2583	3.45
		137	12.22
		1222	
20 59	440.3	17	7.10
		6850	
20 60	436.8	35	8.14
		892	
20 61	428.0	79	7.12
		467	
20 62	439.3	72	3.33
		183	
21 58	435.3	26	1.28
		747	3.43
		39	9.11
		4282	
21 59	431.3	84	3.98
		258	39.39
		724	
21 60	429.7	22	4.19
		992	
21 61	426.2	66	7.03
		535	
21 63	454.7	73	1.04
		1640	
22 57	460.2	302	10.92
		2061	
22 58	449.2	289	4.74
		550	

TABLE A.3 Cont.

Nodal Coordinates	Surface Elevation (meters above msl[a])	Layer Resistivity (Ω-m)	Layer Thickness (m)
22 59	440.6	133	3.05
		3669	1.21
		350	
22 60	426.6	66	3.05
		220	1.22
		397	
22 61	425.0	56	5.95
		147	6.23
		521	
22 62	437.6	261	1.69
		1044	13.64
		509	
23 58	451.4	260	24.34
		3258	
23 59	440.9	124	2.05
		6109	1.92
		8	1.12
		1142	
23 60	426.9	46	13.68
		1222	
23 61	423.5	63	2.47
		122	16.70
		657	
24 58	453.6	659	8.29
		2457	8.10
		25	
24 59	441.0	103	4.76
		2983	11.29
		83	
24 60	431.0	312	0.81
		1271	1.55
		480	
24 61	420.8	26	1.66
		161	12.14
		826	

TABLE A.3 Cont.

Nodal Coordinates	Surface Elevation (meters above msl[a])	Layer Resistivity (Ω-m)	Layer Thickness (m)
25 58	450.4	139	11.11
		734	
25 59	437.8	164	3.85
		600	
25 60	429.7	134	5.82
		2565	14.90
		11	
26 55	445.7	59	5.62
		505	
26 57	453.5	59	8.25
		3111	
26 58	443.5	26	5.12
		942	
26 59	434.8	27	6.27
		1226	
26 60	428.1	71	7.28
		465	12.58
		4679	
27 54	440.2	29	11.52
		1648	
27 56	435.1	30	10.80
		2038	
27 58	437.4	23	4.96
		687	
27 60	422.2	11	1.39
		576	
28 53	436.9	29	6.76
		515	
28 54	434.9	28	3.92
		71	14.05
		665	
28 55	437.8	37	9.22
		417	

TABLE A.3 Cont.

Nodal Coordinates	Surface Elevation (meters above msl[a])	Layer Resistivity (Ω-m)	Layer Thickness (m)
28 56	432.2	27 415	6.59
28 57	433.4	36 279	5.75
28 58	432.4	22 561	4.91
28 59	425.0	18 255 5364	2.54 33.57
29 53	431.5	29 109 1364	3.89 34.75
29 54	430.5	33 379	8.81
29 55	434.8	27 472	6.17
29 56	430.1	40 452	8.41
29 57	430.1	18 582	6.07
29 58	429.2	17 2536	7.05
29 59	421.0	29 800	5.53
30 54	425.5	22 90 1565	2.13 24.21
30 55	429.6	39 488	7.91
30 56	426.1	102 392	8.30
30 57	422.3	92 512	13.77

TABLE A.3 Cont.

Nodal Coordinates	Surface Elevation (meters above msl[a])	Layer Resistivity (Ω-m)	Layer Thickness (m)
30 58	426.9	26	5.10
		192	25.18
		2041	
30 59	419.0	64	7.97
		702	
31 53	426.7	56	9.68
		424	
31 54	428.6	61	12.15
		313	
31 55	419.3	84	4.46
		208	
31 57	419.5	111	8.65
		460	
31 58	417.9	43	4.39
		571	
31 59	416.4	87	4.97
		375	
32 54	423.7	46	6.19
		291	
32 55	432.3	138	2.95
		699	6.72
		131	
32 56	431.0	43	2.76
		479	
32 57	420.7	361	7.18
		1146	11.86
		96	
32 58	411.1	6	1.02
		103,054	
32 59	403.6	20	0.43
		12,616	0.54
		33	

TABLE A.3 Cont.

Nodal Coordinates	Surface Elevation (meters above msl[a])	Layer Resistivity (Ω-m)	Layer Thickness (m)
33 54	432.1	55	6.13
		2680	2.20
		107	36.03
		1319	
33 55	428.8	38	9.70
		427	
33 56	433.2	77	4.05
		317	
33 57	425.4	28	6.29
		509	
33 58	442.0	266	10.73
		417	
33 59	415.7	238	13.30
		552	
34 55	442.2	24	6.59
		324	
34 57	430.4	51	5.19
		362	
34 58	425.1	67	7.81
		773	
35 55	442.2	158	14.49
		597	
35 57	435.2	18	1.56
		485	
35 58	429.2	25	4.54
		1133	
36 57	437.3	67	12.71
		5085	
36 59	438.7	154	5.89
		48	6.21
		5710	
37 57	442.8	196	30.49
		812	

TABLE A.3 Cont.

Nodal Coordinates	Surface Elevation (meters above msl[a])	Layer Resistivity (Ω-m)	Layer Thickness (m)
37 58	443.2	159 11,068	34.06
38 57	447.9	18 377	2.99
38 58	442.4	41 233	7.03
39 56	454.9	16 403	1.47
39 57	449.6	17 206	1.40
40 56	458.7	58 583	4.53

[a] msl = mean sea level.

TABLE A.4 Results of Inversion of Seismic Refraction Profiling Data

Shot Point	Coordinates		Surface Elevation (meters above msl[a])	Layer Velocity (m/s)	Layer Thickness (m)
1029 W	3.00	60.01		666	9.21
				1415	
1030 W	4.00	59.00	451.8	500	4.83
				1290	6.00
				1559	
1031 E	5.04	59.00	443.4	500	4.88
				1290	10.75
				2559	
1033 E	7.12	60.00	446.5	555	5.27
				2696	
1034 N	8.00	60.01	441.0	260	2.05
				693	6.61
				3092	
1035 S	8.00	59.60	439.3	260	1.76
				693	9.46
				3092	
1036 SE	10.90	59.10	447.5	416	4.24
				1536	
1037 NW	10.50	59.60	447.2	416	9.47
				1536	
1038 N	2.00	59.65	483	357	6.16
				1403	
1040 S	2.00	59.00	483.1	357	2.94
				1403	
1041 E	14.00	61.96	459.1	500	12.89
				1515	
1042 W	13.50	61.75	463	500	7.70
				1515	
1043 S	11.90	59.13	441.8	416	6.06
				3354	
1044 N	12.00	59.65	444.0	416	8.80
				3354	

TABLE A.4 Cont.

Shot Point	Coordinates		Surface Elevation (meters above msl[a])	Layer Velocity (m/s)	Layer Thickness (m)
1045 E	13.30	59.50	440.5	250	1.37
				633	11.60
				1660	
1046 W	12.70	59.50	442	250	1.63
				633	10.90
				1660	
1047 E	15.35	60.00	437	400	11.25
				3818	
1048 W	14.31	60.00	440	400	6.86
				3818	
1049 W	17.82	61.00	432	600	10.64
				1514	21.86
				3713	
1050 E	18.85	61.00	430	600	9.76
				1514	12.76
				3713	
1051 W	21.02	61.00	426.2	500	5.00
				1397	15.18
				3788	
1052 E	22.00	60.00	424.5	500	6.64
				1397	15.02
				3788	
1053 E	24.92	61.00	419.5	400	5.19
				1968	17.48
				4115	
1054 W	23.90	61.00	420.8	400	7.02
				1968	14.49
				4115	
1055 NW	28.00	60.40	413	500	7.30
				1738	8.71
				3815	
1056 SE	29.00	59.80	411	500	4.95
				1738	13.45
				3815	

TABLE A.4 Cont.

Shot Point	Coordinates		Surface Elevation (meters above msl[a])	Layer Velocity (m/s)	Layer Thickness (m)
1057 E	31.40	59.80	408.6	500 1817 4723	6.24 13.03
1058 W	30.40	59.80	410.0	500 1817 4723	7.02 9.18
1059 SE	31.50	57.50	410	500 1977 4233	3.87 18.93
1060 NW	31.30	58.50	410	500 1977 4233	3.82 21.93
1061 NE	31.48	53.76	427	555 1179	2.84
1062 SW	31.08	52.84	427	555 1179	6.80
1063 S	31.14	55.14	420	500 2787	6.84
1064 N	30.60	56.08	423	500 2787	6.97
1067 NE	31.00	49.00	-	338 1276	5.59
1068 SW	30.48	48.10	-	338 1276	6.20
1069 W	17.00	61.96	443.5	690 3882	12.29
1070 E	18.05	62.00	440.8	690 3882	9.86
1071 W	16.96	61.00	432.2	555 3128	8.71

TABLE A.4 Cont.

Shot Point	Coordinates		Surface Elevation (meters above msl[a])	Layer Velocity (m/s)	Layer Thickness (m)
1072 E	18.00	61.00	430.3	555 3128	9.58
1073 W	17.00	60.06	437.2	550 2924	6.27
1074 E	18.00	60.00	435.3	550 2924	8.75
1075 W	16.80	63.00	456.9	544 2967	9.41
1076 E	17.80	63.16	456.0	544 2967	11.05
1081 E	18.04	59.00	444.5	652 2044	8.55
1082 W	16.96	58.00	459.5	555 1997	5.36
1083 E	18.00	57.98	453.0	555 1997	10.68
1084 W	33.00	54.52	431	454 1333 3822	7.84 15.26
1086 E	26.02	60.00	428.1	666 3902	14.43
1087 W	24.98	60.02	429.7	666 3902	11.10
1088 W	24.97	59.02	437	454 3005	8.46
1089 E	26.01	59.02	437	454 3005	9.11
1090 W	25.02	58.00	450.4	500 1230 2932	4.84 17.88
1092 E	26.05	58.00	443.5	500 1230 2932	7.43 15.81

TABLE A.4 Cont.

Shot Point	Coordinates		Surface Elevation (meters above msl[a])	Layer Velocity (m/s)	Layer Thickness (m)
1093 E	6.92	61.00	461	750 3159	9.05
1094 W	5.86	61.00	466	750 3159	9.70
1095 W	6.02	59.00	455.9	500 1428 3705	5.06 14.38
1096 E	6.90	59.00	452.8	500 1428 3705	2.93 7.41
1097 W	6.00	57.99	462.5	500 3545	6.17
1098 E	7.00	57.92	460.9	500 3545	5.54
1099 S	35.02	57.00	435.2	500 2320	6.01
1100 N	35.00	58.04	429.2	500 2320	9.58
1101 S	34.02	57.00	430.4	500 1723 3855	5.79 16.66
1102 N	34.02	58.00	425.1	500 1723 3855	5.74 22.29
1103 N	33.02	58.00	422.8	677 2968	8.46
1104 S	33.00	56.98	425.4	677 2968	10.30
1105 S	32.00	57.50	415	633 2716	6.62
1106 N	32.00	58.50	409	633 2716	7.90

TABLE A.4 Cont.

Shot Point	Coordinates		Surface Elevation (meters above msl[a])	Layer Velocity (m/s)	Layer Thickness (m)
1107 E	30.00	57.84	426.9	555 997 3700	5.69 13.50
1108 W	28.97	58.00	429.2	555 997 3700	4.13 15.50
1109 E	30.01	59.00	419	588 2702	7.70
1110 W	28.97	59.00	421	588 2702	7.42
1111 E	28.02	59.00	425	555 1647 6210	7.51 19.10
1112 W	26.98	59.00	430.7	555 1647 6210	5.23 24.66
1113 W	27.00	58.01	437.4	555 1514 4364	8.06 15.40
1114 E	28.02	58.00	432.4	555 1514 4364	6.65 21.36
1115 E	11.00	58.02	444.2	434 1581 3655	5.48 16.97
1116 W	9.96	58.00	448.4	434 1581 3655	5.74 16.84
1117 E	10.04	59.00	450.4	400 3103	5.54
1118 W	9.00	58.99	451.9	400 3103	8.61
1119 N	13.00	57.03	443.3	400 3130	7.98

TABLE A.4 Cont.

Shot Point	Coordinates		Surface Elevation (meters above msl[a])	Layer Velocity (m/s)	Layer Thickness (m)
1120 S	12.98	55.99	447.3	400 3130	5.76
1121 S	13.12	58.00	440.4	346 1665 7492	4.08 35.73
1122 N	13.02	59.00	439	346 1665 7492	8.05 13.39
1123 W	12.60	60.32	447	666 2665	6.16
1124 E	13.64	60.32	443	666 2665	10.41
1125 W	13.01	61.00	456.7	500 1219 3663	3.31 20.03
1126 E	14.05	61.00	449.8	500 1219 3663	6.57 8.72
1127 E	12.42	61.00	464.9	588 1574 3491	5.67 15.42
1128 W	11.38	61.00	464.9	588 1574 3491	3.52 20.84
1129 W	21.98	58.98	440.6	625 1561 5873	4.63 29.71
1130 E	23.02	59.00	440.9	625 1561 5873	5.49 26.99
1131 E	23.00	60.01	426.9	500 7646	13.59
1132 W	22.03	59.98	426.6	500 1536	3.92

TABLE A.4 Cont.

Shot Point	Coordinates		Surface Elevation (meters above msl[a])	Layer Velocity (m/s)	Layer Thickness (m)
1133 W	21.99	58.00	449.2	544	3.24
				1256	36.08
				4696	
1134 E	23.03	58.00	451.4	544	5.68
				1256	20.97
				4696	
1135 N	21.02	58.00	435.3	500	6.87
				3002	
1136 S	21.00	57.00	432	500	9.90
				3002	

[a] msl = mean sea level.

Appendix B:

Visualizations of Some of the Results from the Geophysical Surveys in the Lautertal

Appendix B: Visualizations of Some of the Results from the Geophysical Surveys in the Lautertal

Introduction

The figures on the following pages are three-dimensional representations of some of the geophysical data obtained in studies of the Lautertal at Hohenfels, Germany. Each figure is preceded by an explanation of the information portrayed and the color convention used.

Figure B.1

Figure B.1A shows, in plan view, the locations where electromagnetic readings were made in the Lautertal. These locations correspond to nodes of an orthogonal grid (with nodal spacing of 125 m) covering the Lautertal.

Figures B.1B-D show electrical conductivity distributions corresponding to transmitter-receiver spacings of 10, 20, and 40 m, respectively, superimposed on the surface topography of the Lautertal (vertical exaggeration of 10). A conductivity value obtained from a given transmitter-receiver spacing is the weighted average of the conductivities of the rocks from the earth's surface to a depth approximately equal to the transmitter-receiver spacing.

The blue color in Figures B.1B-D corresponds to areas where the near-surface deposits have predominantly high conductivity, with the purple color associated with the highest conductivities. The yellow color corresponds to areas where the near-surface deposits have predominantly low conductivity. The higher conductivity values indicate the presence of fine-grained, unconsolidated surficial deposits, which are capable of retaining water, and/or coarse-grained alluvium saturated with water. The lower conductivity values indicate the presence of well-drained, coarse alluvium and/or carbonate bedrock.

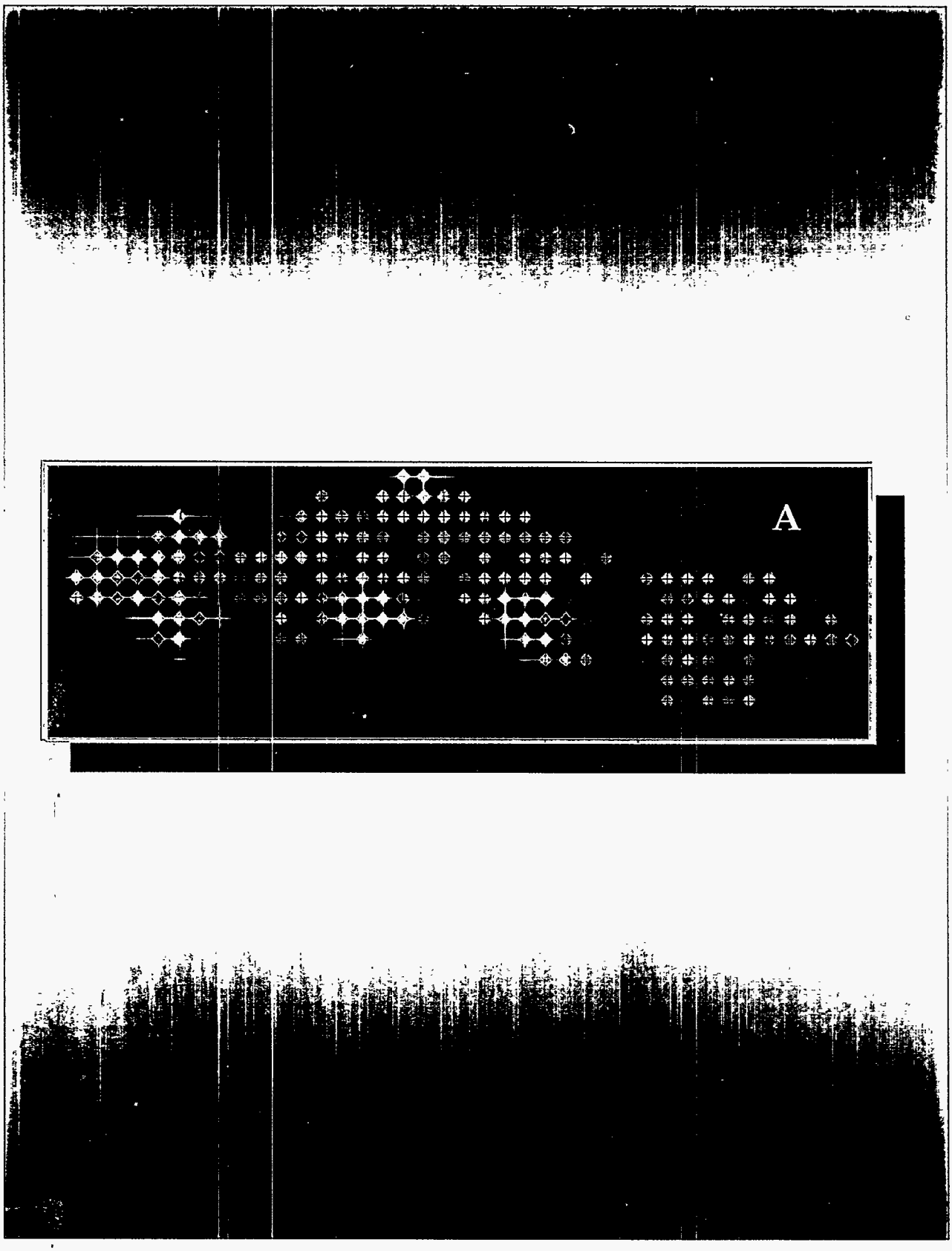

FIGURE B.1 Electrical Conductivity Distributions in the Lautertal as Determined by Electromagnetic Surveying

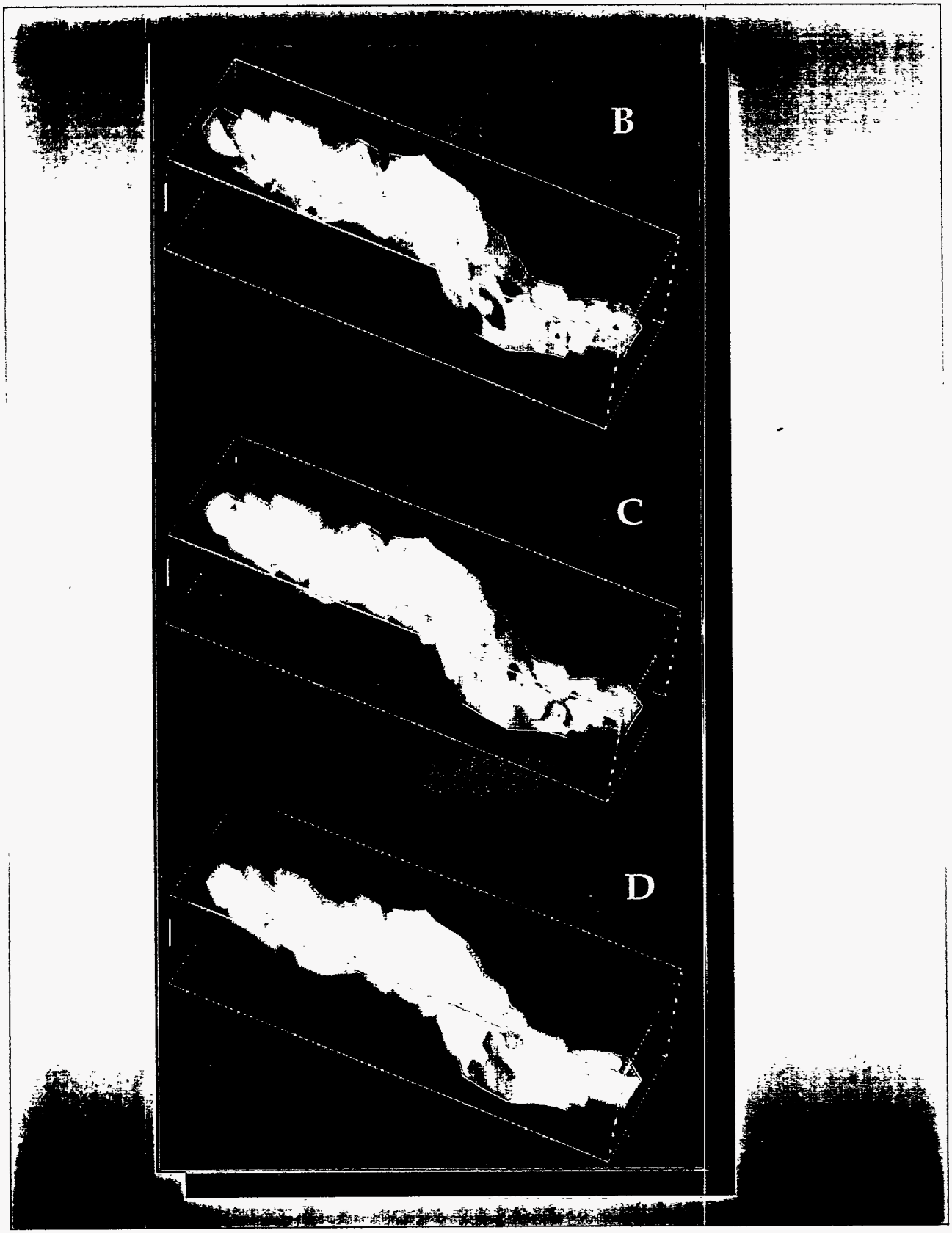

FIGURE B.1 (Cont.)

Figure B.2

Figure B.2A shows, in plan view, the locations where vertical electrical soundings were made in the Lautertal. The locations correspond to nodes of an orthogonal grid (with nodal spacing of 125 m) covering the Lautertal.

Figure B.2B shows a three-dimensional view (looking to the northwest) of the near-surface deposits in the Lautertal (vertical exaggeration of 10) based on vertical electrical soundings. The orange dots correspond to the top of the fine-grained, unconsolidated surficial deposits (loam and loess); the yellow dots correspond to the top of the coarse-grained, unconsolidated deposits (alluvium); and the purple dots correspond to the top of the carbonate bedrock.

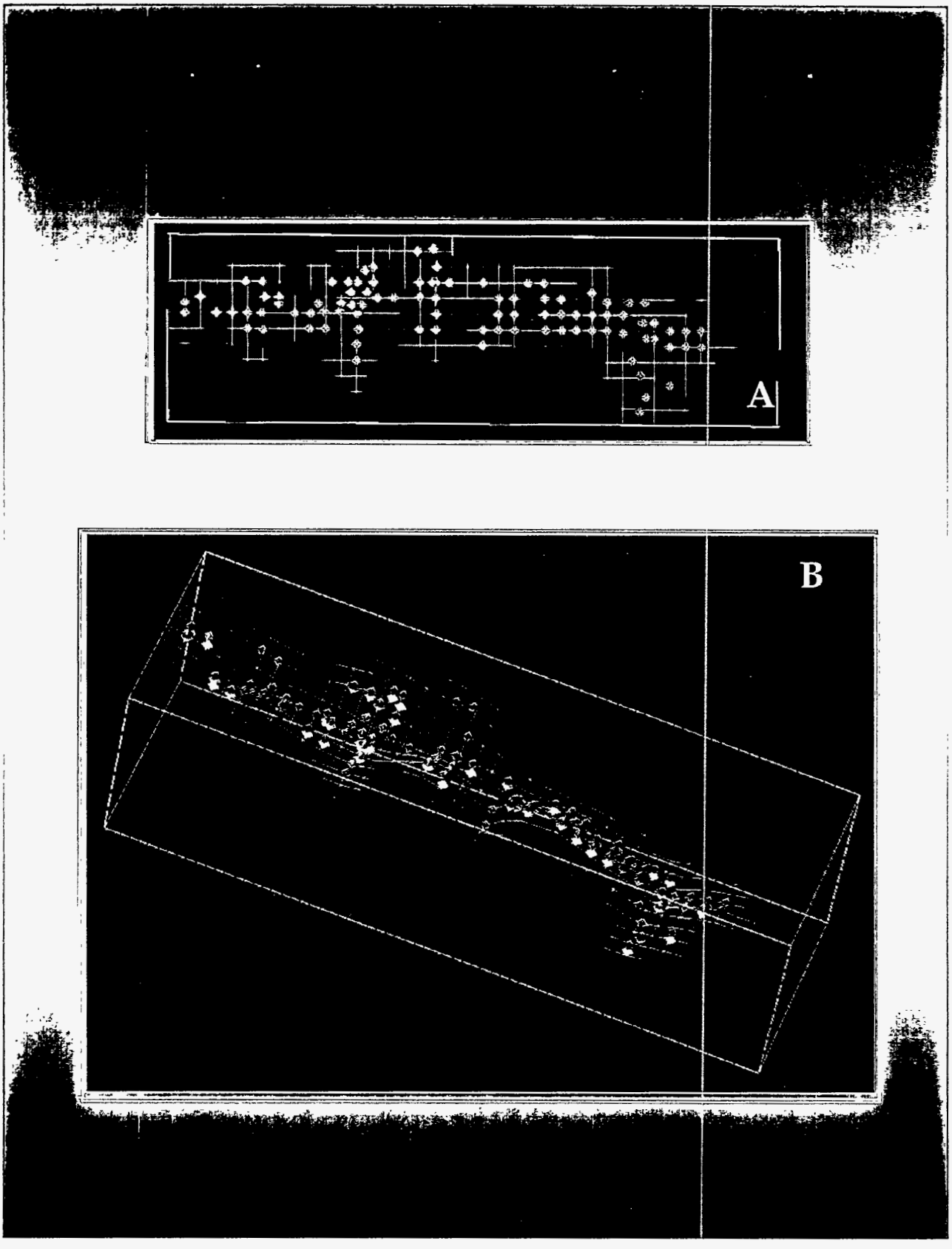

FIGURE B.2 Shallow Geological Framework of the Lautertal as Determined by Vertical Electrical Soundings

Figure B.3

Figure B.3A shows, in plan view, the locations of the shot points employed in the seismic refraction profiling in the Lautertal and the nature of the deposits immediately below the fine-grained, unconsolidated surficial deposits (loam and loess) based on seismic refraction profiling. The yellow color indicates those areas where the loam and loess lie on coarse-grained, unconsolidated deposits (alluvium), and the purple color indicates those areas where the loam and loess lie on the carbonate bedrock.

Figure B.3B shows a three-dimensional view (looking to the northwest) of the surface topography and the base of the loam and loess in the Lautertal (vertical exaggeration of 10). The surface topography is indicated by the shot point locations. The base of the loam and loess is shown in yellow and purple. The color convention is the same as that used in Figure B.3A.

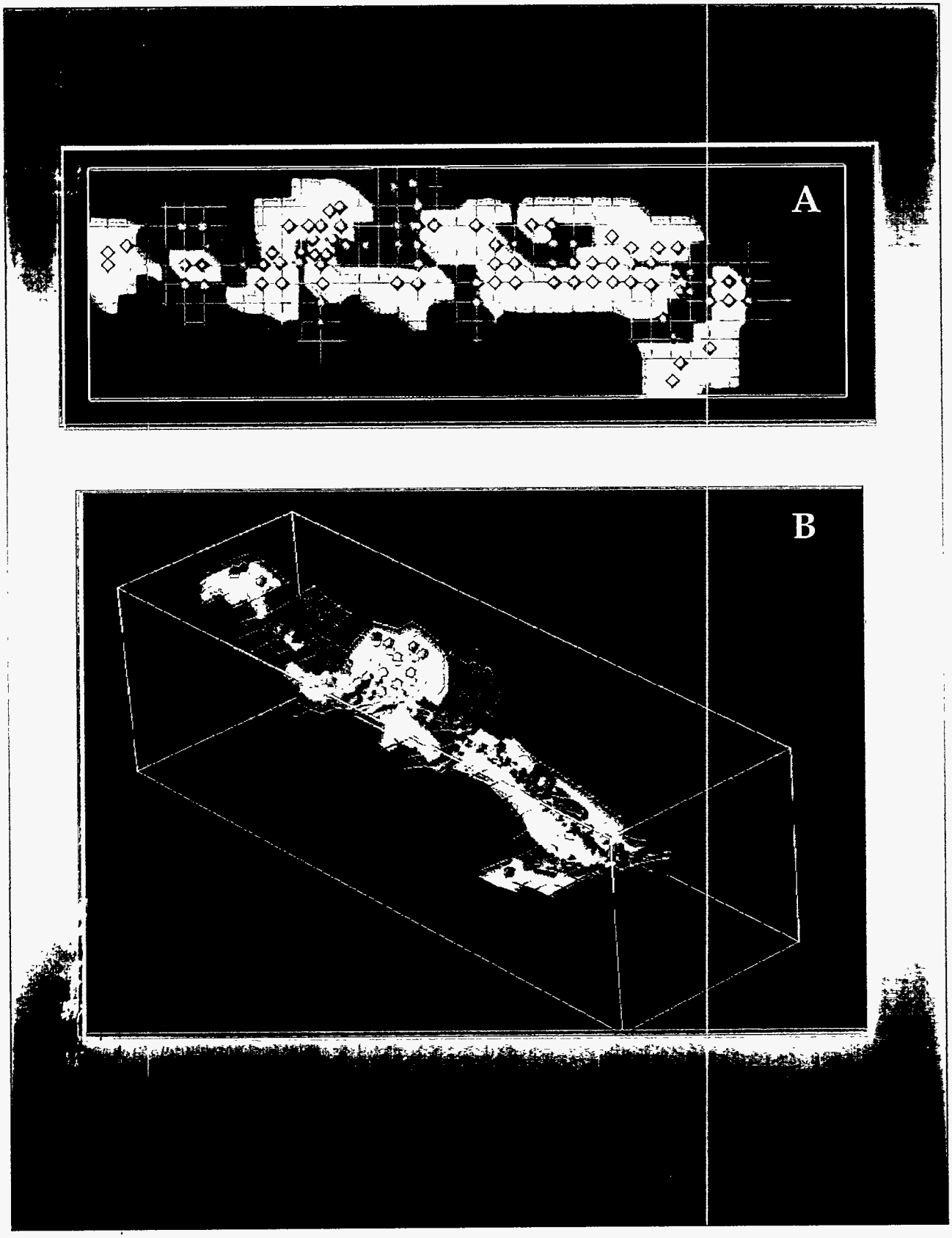

FIGURE B.3 Surface Topography and Base of the Fine-Grained, Unconsolidated Surficial Deposits (Loam and Loess) in the Lautertal

Figure B.4

Figure B.4A shows, in plan view, the locations of the shot points employed in the seismic refraction profiling in the Lautertal. These locations generally correspond to nodes of an orthogonal grid (with nodal spacing of 125 m) covering the Lautertal.

Figure B.4B shows a three-dimensional view (looking to the northwest) of the near-surface deposits in the Lautertal (vertical exaggeration of 10) based on seismic refraction profiling. The orange dots correspond to the top of the fine-grained, unconsolidated surficial deposits (loam and loess); the yellow dots correspond to the top of the coarse-grained, unconsolidated deposits (alluvium); and the purple dots correspond to the top of the carbonate bedrock.

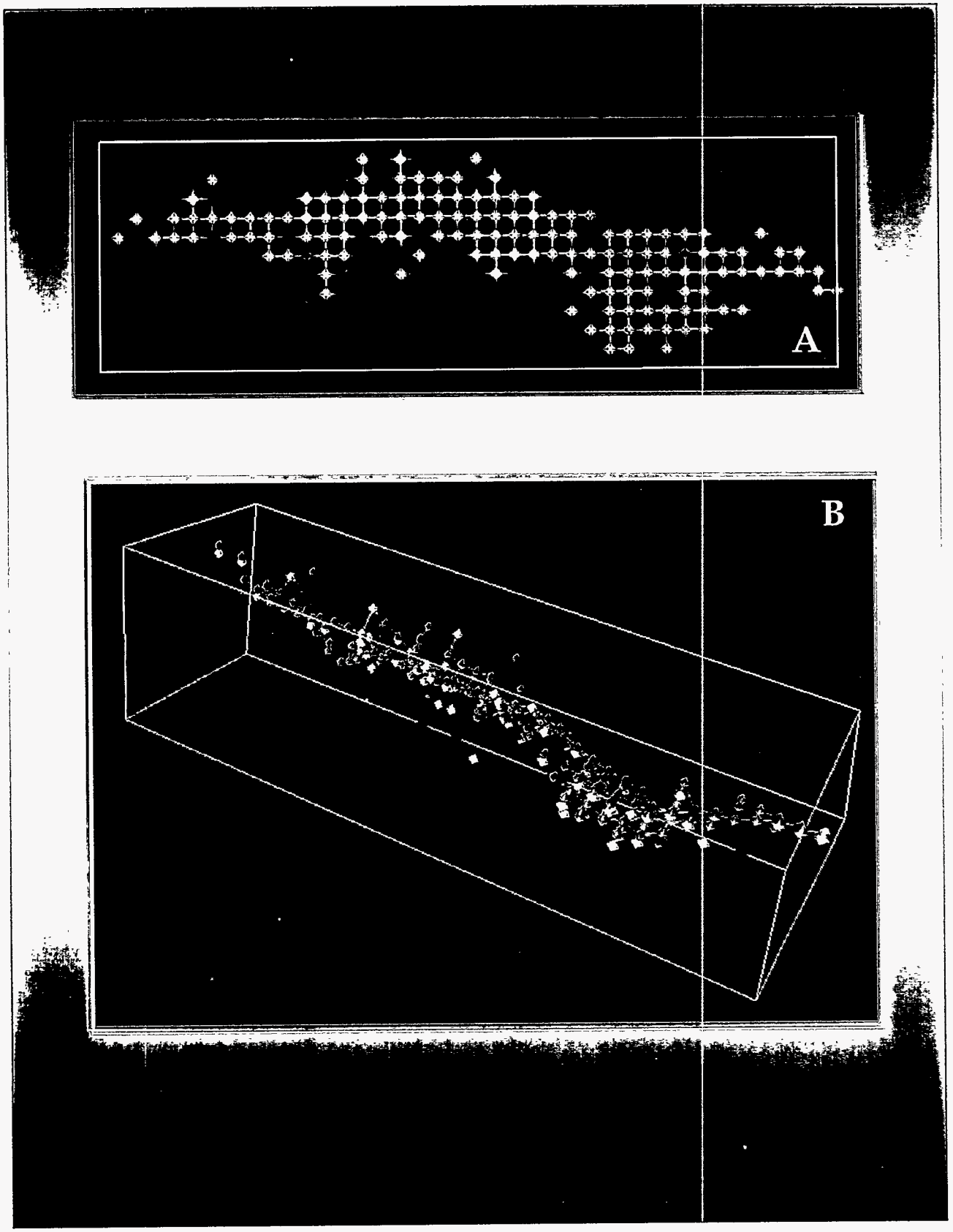

FIGURE B.4 Shallow Geological Framework of the Lautertal as Determined by Seismic Refraction Profiling